

Fluctuations of the heat exchanged between two quantum spin chains

Gabriel T. Landi*

Universidade Federal do ABC, 09210-580 Santo André, Brazil

(Dated: November 1, 2018)

We analyze the statistics of the heat which flows between two quantum XX spin chains initially prepared at different temperatures. A perturbative approach is developed which enable us to find the characteristic function of the heat for arbitrary system sizes, from which the probability of heat is computed numerically. Hence, we are able to examine the role of the thermodynamic limit in this non-equilibrium setting. We also study the average heat as a function of time and find that finite systems never thermalize. Conversely, thermalization does occur in the thermodynamic limit, for which an exact expression for the average heat is obtained. Finally, using the same formal framework, we also compute the distribution of the work performed by an external agent when turning on the interaction between the two chains. We also find that all of the above thermodynamic quantities are extremely sensitive to the quantum phase transition of the XX chain.

I. INTRODUCTION

When studying the thermodynamic properties of microscopic systems (quantum or classical), it is found that quantities such as heat, work and entropy production may fluctuate between each realization of an experiment. They should therefore be interpreted as random variables described by a probability distribution. Over the past two decades, researchers have discovered that these distributions obey certain symmetry relations which touch deeply into the nature of irreversibility and the arrow of time [1, 2]. These relations are now generally known as fluctuation theorems [3–27] and constitute the most important advance thus far in non-equilibrium thermodynamics. Historically, fluctuation theorems were initially developed for classical systems obeying either Hamiltonian or stochastic dynamics [3–13]. Their validity was also extensively verified experimentally [28–31]. Conversely, their development for quantum systems is much more recent [14–27], including their experimental verification [32]. In fact, studying the thermodynamic properties of small quantum systems constitutes one of the major programs nowadays in non-equilibrium statistical mechanics. It is hoped that this will lead to a deeper understanding of irreversible phenomena which, besides being of great value by itself, will also help advance many other areas, ranging from quantum information [33–36] to biology [37].

The probability distributions of heat, work and entropy production are the central objects in the theory of non-equilibrium fluctuations and quantum thermodynamics. Hence the importance of computing them in the context of specific examples, either theoretically [38–46] or experimentally [2, 28–32]. However, this may be a challenging task, even for problems which can be exactly diagonalized. This difficulty is aggravated further for quantum many-body systems, due to the complex nature of the energy spectrum and the enormous num-

ber of transitions allowed between these levels. Notwithstanding, it is essential that these problems be addressed, for they provide a key insight into the workings of non-equilibrium phenomena. Particularly important is the ability to analyze systems with variable size. Unlike in equilibrium statistical mechanics, the role of the thermodynamic limit in non-equilibrium fluctuations is much more intricate and to this date largely unexplored.

In this paper we will be mostly concerned with the statistics of the heat which flows between two systems prepared at different temperatures. Heat fluctuations in quantum systems has recently been the subject of a large number of studies [47–59]. The setup considered here is that proposed by Jarzynski and Wójcik [11]. Suppose we initially have two systems prepared at different temperatures T_1 and T_2 by placing them in contact with thermal reservoirs. At $t = 0$ we unplug them from their baths and put them in contact with each other, thus allowing for heat to flow between the two bodies. According to the second law of thermodynamics, heat should always flow from the hotter system to the colder [60]. Moreover, we know from classical thermodynamics that this flow will continue until the two systems reach thermal equilibrium at a common temperature T^* . If U_1 and U_2 are the internal energies of each system then, due to the monotonically increasing dependence of the energy on temperature, the condition for equilibrium is tantamount to $U_1(T^*) = U_2(T^*)$. The value of T^* is then fixed from conservation of energy:

$$2U_1(T^*) = U_1(T_1) + U_2(T_2) \quad (1)$$

Moreover, the total heat which entered the first body in the interval from $t = 0$ to $t = \infty$ is

$$Q = \frac{U_2(T_2) - U_1(T_1)}{2} \quad (2)$$

The situation is entirely different if the two systems are not macroscopically large. In this case, when we unplug them from their reservoirs at $t = 0$, the observed thermal states may fluctuate substantially from their average values. Hence, the heat which flows between the two bodies

* gtlandi@gmail.com

will now be a random quantity. In quantum systems, we also have an additional source of randomness due to the intrinsic quantum fluctuations. Due to both types of fluctuations, it becomes possible to observe a heat flow in the opposite direction, from the colder system to the hotter. Let us denote by $P_t(Q)$ the probability that a certain amount of heat Q entered system 1 after a time t . In Ref. [11] Jarzynski and Wójcik showed that $P_t(Q)$ obeys the following fluctuation theorem:

$$\frac{P_t(Q)}{P_t(-Q)} = e^{\Delta\beta Q} \quad (3)$$

where $\Delta\beta = \frac{1}{T_1} - \frac{1}{T_2}$. This relation was derived under the assumption of *weak coupling*; i.e., that the energy between the two systems is small compared to their individual energies. This means that the energy which enters system 1 is, to a good approximation, the same as the energy which left system 2.

Eq. (3) may be physically interpreted as saying that it is exponentially more likely that heat will flow in the right direction. Of course, since Q is an extensive quantity, for macroscopic bodies the probability of heat flowing in the opposite direction is negligible. From Eq. (3) it also follows that Q obeys a non-equilibrium equality:

$$\langle e^{-\Delta\beta Q} \rangle_t = 1 \quad (4)$$

Using Jensen's inequality and assuming that $T_2 > T_1$, this leads to

$$\langle Q \rangle_t \geq 0 \quad (5)$$

In the absence of work the second law states that heat flows from hot to cold. This equation may be seen as a generalization of this law, valid also for microscopic bodies. Essentially, it says that *on average* heat flows from hot to cold. Another interesting fact about Eq. (3) is that it holds whether or not the two systems actually thermalize. In fact, since the evolution for $t > 0$ is unitary, it is expected that for finite systems the heat will oscillate indefinitely, back and forth between the two bodies. That is, $\langle Q \rangle_t$ may never approach Q in Eq. (2) as $t \rightarrow \infty$. Conversely, we expect from everyday experience that in the thermodynamic limit the two systems should thermalize.

Some remarks about the present setup are in place. First, we note that a proposal to experimentally measure the statistics of heat in a quantum system was recently given in Ref. [59]. The statistics of heat is also intimately related to Landauer's principle [61]. In quantum systems, this highlights the important connection between quantum thermodynamics and quantum information [27]. Finally, we note that by turning on the interaction at time $t = 0$, work must be performed by an external agent. This work is also a random quantity described by its own probability distribution [62].

The primary motivation behind this paper is to establish a framework to study the distribution of thermodynamic quantities for quantum many-body systems. To

accomplish this we shall study the Jarzynski and Wójcik setup for the case of two XX quantum spin chains connected by an XX coupling. This model is exactly diagonalizable in terms of Fermionic operators. Notwithstanding, it will be shown that computing the distribution $P_t(Q)$ for arbitrary sizes is still impossible due to the enormous number of transitions inherent of a many-body problem. Instead we shall adopt a different route and exploit the fact that, if the size of the two chains is moderately large, the coupling between them will be comparatively much smaller so that we may apply perturbation theory to the interaction potential. The perturbation parameter will be shown to be proportional to g_0/N , where g_0 is the coupling constant between the two chains and N are their individual sizes. Hence, the coupling constant itself does not need to be necessarily small. All we require is that N is sufficiently large. Moreover, the correctness of the approximation will improve as we increase the size of the systems and, in particular, it will become *exact* in the thermodynamic limit.

Our main focus will be on the distribution of the heat which flows between the two systems $P_t(Q)$ and on the average heat $\langle Q \rangle_t$ as a function of time. However, we will also discuss the statistics of the work that must be performed by an external agent in turning on the interaction at $t = 0$. It will be shown that even using the above mentioned perturbative approach, finding these distributions explicitly is still an intractable problem. For, even in this case, the number of transitions is still enormous (the problem is essentially one of bookkeeping). Our approach will then be to compute the characteristic function which is much simpler and, from it, obtain the probability distributions either numerically or, in certain cases, analytically. The average heat, on the other hand, will be shown to have a very simple formula which becomes exact in the thermodynamic limit.

It will be shown that all thermodynamic quantities are extremely sensitive to the quantum phase transition that the XX chain undergoes as a function of the magnetic field [63]. Moreover, it will be shown that finite systems never thermalize. The average heat $\langle Q \rangle_t$ is a well behaved function of time up to a certain point, after which violent oscillations start and never cease. However, as the size increases, the instant where this transition occurs is shifted to larger and larger times. Consequently, in the thermodynamic limit the two systems do thermalize and $\langle Q \rangle_t$ tends to Q as $t \rightarrow \infty$.

While we will be concerned with a specific system, the methodology presented here is quite general and may be used to study the distribution of any thermodynamic quantity in a broad variety of situations. For instance, we note the connection between the present problem and that studied in Ref. [64]. It is also worth noting that the equivalence between the XX chain and the Tonks-Girardeau model [65] means that the present results can in principle be verified experimentally, for instance using Rubidium atoms [66, 67].

II. FORMAL FRAMEWORK

A. System setup

We consider here the physical setup proposed by Jarzynski and Wójcik [11]. Initially we have two systems with Hamiltonians H_1 and H_2 . For simplicity we assume that both have the same energy spectrum so that

$$H_1|n_1\rangle = E_{n_1}|n_1\rangle \quad (6)$$

$$H_2|n_2\rangle = E_{n_2}|n_2\rangle \quad (7)$$

The two systems have been prepared in thermal equilibrium at different temperatures T_1 and T_2 . Then, at $t = 0^-$, we unplug them from their reservoirs and measure their state. The density matrix of the composite system is

$$\rho_{\text{th}} = \frac{e^{-\beta_1 H_1}}{Z_1} \frac{e^{-\beta_2 H_2}}{Z_2} \quad (8)$$

where $\beta_{1,2} = 1/T_{1,2}$ ($k_B = 1$) and $Z_{1,2}$ are the corresponding partition functions. Hence, the probability of obtaining the state $|\mathbf{n}\rangle = |n_1, n_2\rangle$ is

$$p_{\mathbf{n}} = \frac{e^{-\beta_1 E_{n_1}}}{Z_1} \frac{e^{-\beta_2 E_{n_2}}}{Z_2} \quad (9)$$

Immediately after this measurement, at $t = 0^+$, we turn on an interaction V between the two systems (i.e., we perform a quantum quench). Consequently, the total Hamiltonian passes from

$$H_0 = H_1 + H_2 \quad (10)$$

at $t = 0^-$ to

$$H = H_1 + H_2 + V \quad (11)$$

at $t = 0^+$. The eigenbasis of H_0 is $|\mathbf{n}\rangle = |n_1, n_2\rangle$ whereas the eigenbasis of H is denoted by $|f\rangle$, where

$$H|f\rangle = \mathcal{E}_f|f\rangle \quad (12)$$

The process of connecting the two systems obviously occurs during a finite time τ_V over which the interaction is ramped up from 0 to V . However, we assume that τ_V is much shorter than the typical evolution time of the systems so that, to a good approximation, we may take this process to be instantaneous. Notice that this process changes the energy of the system and thus requires the expenditure of work by an external agent. Moreover, being a sudden quench, this is the extreme case of an irreversible process.

After we turn on the interaction the system will evolve unitarily in time under the total Hamiltonian H given by Eq. (11). If at some instant of time t we measure the total energy H and find a value \mathcal{E}_f , then the difference between this value and the total energy $E_{n_1} + E_{n_2}$ of the

first measurement must be attributed to the work performed by the external agent, since the composite system is isolated. Thus, the work performed is

$$W = \mathcal{E}_f - (E_{n_1} + E_{n_2}) \quad (13)$$

The instant where this second measurement takes place is unimportant since the evolution is unitary.

Since the two systems were prepared at different temperatures, energy will also flow from one system to the other in the form of heat. A measurement of H is incapable of yielding information about this process. To examine it, we must individually measure the observables H_1 and H_2 . Suppose that at a certain time t we perform such measurement and obtain the state $|\mathbf{m}\rangle = |m_1, m_2\rangle$. Then the energy change in each system is, by definition,

$$Q_1 = E_{m_1} - E_{n_1} \quad (14)$$

$$Q_2 = E_{m_2} - E_{n_2} \quad (15)$$

Unlike W , the values of Q_1 and Q_2 depend on the time t at which the second measurement was performed. Note, though, that it is in general incorrect to interpret Q_1 and Q_2 as the heat which entered each system, since part of this energy change may also be due to the work performed by the external agent. Such interpretation will only be true in the *weak coupling limit*, in which case we expect that

$$Q_1 \simeq -Q_2 := Q$$

In this case we may say that Q is the heat which flowed from system 2 toward system 1.

B. Analysis in terms of expectation values

The discussion is made clearer in terms of expectation values. At $t = 0^-$ the average energy of the system was

$$\langle H_0 \rangle_0 = \langle H_1 \rangle_0 + \langle H_2 \rangle_0 = U(T_1) + U(T_2) \quad (16)$$

where $U(T)$ is the internal energy at a temperature T . After the quench, at $t = 0^+$, the average energy of the composite system changes abruptly to

$$\langle H \rangle_0 = \langle H_1 \rangle_0 + \langle H_2 \rangle_0 + \langle V \rangle_0 \quad (17)$$

For $t > 0$ the evolution is unitary so that

$$\langle H \rangle_t = \langle H \rangle_0 \quad (18)$$

where

$$\langle H \rangle_t = \langle H_1 \rangle_t + \langle H_2 \rangle_t + \langle V \rangle_t \quad (19)$$

and the expectation value of any operator \mathcal{O} at time t is, by definition,

$$\langle \mathcal{O} \rangle_t = \text{tr} \{ U^\dagger(t) \mathcal{O} U(t) \rho_{\text{th}} \} = \text{tr} \{ \mathcal{O} \rho(t) \} \quad (20)$$

where $U(t) = e^{-iHt}$ is the time evolution operator.

At any given time t we may define the average work performed by the external agent as

$$\langle W \rangle = \langle H \rangle_t - \langle H_0 \rangle_0 = \langle V \rangle_0 \quad (21)$$

which is thus seen to be independent of time. Similarly, the average change in energy of each system is

$$\langle Q_{1,2} \rangle_t = \langle H_{1,2} \rangle_t - \langle H_{1,2} \rangle_0 \quad (22)$$

From Eqs. (17)-(19) we conclude that

$$\langle Q_1 \rangle_t + \langle Q_2 \rangle_t = \langle V \rangle_0 - \langle V \rangle_t \quad (23)$$

The term $-\langle V \rangle_t$ corresponds to the average work that must be performed if the interaction V is turned off at time t . Hence, the right-hand side of this equation is the total average work that must be performed by an external agent in turning the interaction on at time $t = 0$ and off at time t . If this total work is small then we obtain

$$\langle Q_1 \rangle_t \simeq -\langle Q_2 \rangle_t := \langle Q \rangle_t \quad (24)$$

which means that all the energy which left system 2 enters system 1. In other words, no energy is retained in the interaction V .

C. The statistics of work

In order to obtain the probability distributions of work or heat, two measurements are necessary [19]. One at time $t = 0^-$, before we turn on the interaction, and one at a given time t . We begin with the statistics of the work performed by the external agent in turning on the interaction V , Eq. (13). The conditional probability of finding the system in a state $|f\rangle$ at a time t given that it was at state $|\mathbf{n}\rangle$ at time 0 is $|\langle f|U(t)|\mathbf{n}\rangle|^2$. But since $U(t)|f\rangle = e^{-i\mathcal{E}_f t}|f\rangle$ this reduces to $|\langle f|\mathbf{n}\rangle|^2$. Hence, the probability of work in this case is [23]

$$P(W) = \sum_{\mathbf{n}, f} |\langle f|\mathbf{n}\rangle|^2 p_{\mathbf{n}} \delta[W - (\mathcal{E}_f - (E_{n_1} + E_{n_2}))] \quad (25)$$

The characteristic function may be computed directly from this expression and reads [19]

$$M(u) = \langle e^{iuW} \rangle = \text{tr} \left\{ e^{iuH} e^{-iu(H_1 + H_2)} \rho_{\text{th}} \right\} \quad (26)$$

The characteristic function is thus seen to be much more convenient to work with than the probability distribution since it is simply given by a trace (there is an analogy here with the partition function). The first moment of W in Eq. (21) follows immediately from Eq. (26), as does the second moment:

$$\langle W^2 \rangle = \langle V^2 \rangle_0 + \langle [H_0, V] \rangle_0 \quad (27)$$

This shows clearly that it is not possible to attribute an observable to W . The same will be true for heat.

If the two systems start at the same temperature, $\beta_1 = \beta_2 = \beta$, we may interpret them as a single system in thermal equilibrium with Hamiltonian H_0 . In this case, setting $iu = -\beta$ in Eq. (26) we arrive at the Jarzynski equality [7]

$$\langle e^{-\beta W} \rangle = e^{-\beta \Delta F} \quad (28)$$

where $\Delta F = -T \log \left(\frac{Z}{Z_1 Z_2} \right)$, with Z being the partition function of the system with Hamiltonian H and temperature T . This relation only holds if the temperature of the two systems are initially equal. Continuing with this assumption, we know from classical thermodynamics that

$$\langle W \rangle \geq \Delta F \quad (29)$$

where the equality only holds if the process is reversible. The difference is defined as the irreversible work W_{irr} and is related to the entropy produced in the process by

$$\Sigma_{\text{work}} = \beta W_{\text{irr}} = \beta (\langle W \rangle - \Delta F) \quad (30)$$

Due to fluctuations, in microscopic systems it is possible to observe violations of the inequality (29). With this in mind, it is of interest to define,

$$P(W < \Delta F) = \int_{-\infty}^{\Delta F} P(W) dW \quad (31)$$

This is what would traditionally be called ‘‘probability of second law violations’’ [3], although this nomenclature is not precisely correct since the second law is, by assumption, valid only for macroscopic systems. In the case that $P(W)$ is a probability density function — i.e., provided it does not contain any delta peaks — it is possible to relate $P(W < \Delta F)$ to the characteristic function as

$$P(W < \Delta F) = \frac{1}{2} + \frac{i}{2\pi} \int_{-\infty}^{\infty} \frac{M(u)}{u} e^{-iu\Delta F} du \quad (32)$$

D. The statistics of heat

Next we discuss the stochastic quantities defined in Eq. (14), irrespective of whether or not they may be interpreted as heat. The conditional probability of finding the system in the state $|\mathbf{m}\rangle = |m_1, m_2\rangle$ at time t given that it was initially at $|\mathbf{n}\rangle = |n_1, n_2\rangle$ at time 0 is $|\langle \mathbf{m}|U(t)|\mathbf{n}\rangle|^2$. Hence, the corresponding probability distribution is [11]

$$P_t(Q_1) = \sum_{\mathbf{n}, \mathbf{m}} |\langle \mathbf{m}|U(t)|\mathbf{n}\rangle|^2 p_{\mathbf{n}} \delta[Q_1 - (E_{m_1} - E_{n_1})] \quad (33)$$

with a similar formula for $P_t(Q_2)$. The characteristic function is

$$F_t(r) = \langle e^{irQ_1} \rangle_t = \text{tr} \left\{ U^\dagger(t) e^{irH_1} U(t) e^{-irH_1} \rho_{\text{th}} \right\} \quad (34)$$

Eq. (22) follows immediately from this relation, as well as the second moment of Q_1

$$\langle Q_1^2 \rangle_t = \langle H_1^2 \rangle_t + \langle H_1^2 \rangle_0 - 2 \text{tr} \{ U^\dagger H_1 U H_1 \rho_{\text{th}} \} \quad (35)$$

It is important to note that all these definitions hold whether or not Q_1 may be interpreted as the heat which flowed through the system. The only difference is that, if that is indeed true, then $P_t(Q_1)$ should obey the fluctuation theorem in Eq. (3). Moreover, due to Eq. (4) we should also have $F_t(r = i\Delta\beta) = 1$.

In the case of heat we may also study the ‘‘probability of second law violations’’, which in this case means $P_t(Q < 0)$. Similarly to Eq. (32) we may write

$$P_t(Q < 0) = \frac{1}{2} + \frac{i}{2\pi} \int_{-\infty}^{\infty} \frac{F_t(r)}{r} dr \quad (36)$$

Since $P_t(Q)$ is real, it follows that $F_t(-r) = F_t^*(r)$ so that only the imaginary part of $F_t(r)$ contributes to this formula. If both temperatures are equal, $F_t(r)$ will be real yielding $P_t(Q < 0) = 1/2$, as expected since in this case there is no preferred direction of heat flow.

III. THE MODEL

We now introduce the model which shall be analyzed, namely that of two identical one-dimensional quantum XX spin chains with an XX coupling. Each chain has length N and is described by the usual Pauli matrices. The Hamiltonians H_1 and H_2 , and the interaction potential V , are given by

$$H_1 = \frac{h}{2} \sum_{i=1}^N \sigma_i^z + \frac{J}{2} \sum_{i=1}^{N-1} (\sigma_i^x \sigma_{i+1}^x + \sigma_i^y \sigma_{i+1}^y) \quad (37)$$

$$H_2 = \frac{h}{2} \sum_{i=N+1}^{2N} \sigma_i^z + \frac{J}{2} \sum_{i=N+1}^{2N-1} (\sigma_i^x \sigma_{i+1}^x + \sigma_i^y \sigma_{i+1}^y) \quad (38)$$

$$V = \frac{g_0}{2} (\sigma_N^x \sigma_{N+1}^x + \sigma_N^y \sigma_{N+1}^y) \quad (39)$$

A. Diagonalization of the individual Hamiltonians

We begin by diagonalizing the Hamiltonians H_1 and H_2 individually. To accomplish this we introduce Fermionic operators

$$c_k = \left[\prod_{j=1}^{k-1} (-\sigma_j^z) \right] \sigma_k^- \quad (40)$$

where $\sigma_k^\pm = \sigma_k^x \pm i\sigma_k^y$ and $k = 1, \dots, 2N$. The c_k satisfy the Fermionic commutation relations

$$\{c_k, c_\ell^\dagger\} = \delta_{k,\ell} \quad (41)$$

In terms of these operators Eqs. (37)-(39) become

$$H_1 = h \sum_{k=1}^N c_k^\dagger c_k + J \sum_{k=1}^{N-1} (c_k^\dagger c_{k+1} + c_{k+1}^\dagger c_k) \quad (42)$$

$$H_2 = h \sum_{k=N+1}^{2N} c_k^\dagger c_k + J \sum_{k=N+1}^{2N-1} (c_k^\dagger c_{k+1} + c_{k+1}^\dagger c_k) \quad (43)$$

$$V = g_0 (c_N^\dagger c_{N+1} + c_{N+1}^\dagger c_N) \quad (44)$$

where in H_1 and H_2 we omitted a constant term $Nh/2$, which we henceforth neglect.

We can also write H_1 and H_2 as

$$H_1 = \sum_{k,\ell=1}^N A_{k,\ell} c_k^\dagger c_\ell$$

$$H_2 = \sum_{k,\ell=1}^N A_{k,\ell} c_{k+N}^\dagger c_{\ell+N}$$

where $A_{k,\ell} = h\delta_{k,\ell} + J(\delta_{k,\ell+1} + \delta_{k,\ell-1})$. The matrix A is diagonalized as $A_{k,\ell} = \sum_{n=1}^N x_{k,n} \lambda_n x_{\ell,n}$ where the eigenvalues λ_k and the eigenvectors $x_{k,\ell}$ are

$$\lambda_k = h + 2J \cos\left(\frac{\pi k}{N+1}\right) \quad (45)$$

$$x_{k,\ell} = \sqrt{\frac{2}{N+1}} \sin\left(\frac{\pi k\ell}{N+1}\right) \quad (46)$$

Let us then define a new set of operators according to

$$b_k = \sum_{n=1}^N x_{n,k} c_n, \quad b_{k+N} = \sum_{n=1}^N x_{n,k} c_{n+N} \quad (47)$$

Since the $x_{k,\ell}$ form an orthogonal matrix, these transformations preserve the Fermionic commutation relation (41) for all operators b_k :

$$\{b_k, b_\ell^\dagger\} = \delta_{k,\ell} \quad (48)$$

where $k, \ell = 1, \dots, 2N$. In terms of these new operators the Hamiltonians H_1 and H_2 in Eqs. (42) and (43) are put in diagonal form:

$$H_1 = \sum_{k=1}^N \lambda_k b_k^\dagger b_k \quad (49)$$

$$H_2 = \sum_{k=1}^N \lambda_k b_{k+N}^\dagger b_{k+N} \quad (50)$$

Each chain may thus be viewed as a sum of non-interacting b-fermions.

In terms of the b_k the interaction energy V in Eq. (44) becomes

$$V = \sum_{k,\ell=1}^N G_{k,\ell} (b_k^\dagger b_{\ell+N} + b_{\ell+N}^\dagger b_k) \quad (51)$$

where

$$G_{k,\ell} = \frac{2g_0}{N+1} \sin\left(\frac{\pi N k}{N+1}\right) \sin\left(\frac{\pi \ell}{N+1}\right) \quad (52)$$

Eq. (51) has a simple physical interpretation. Each term in V destroys a b-fermion in one chain and creates a b-fermion in the other chain, a process which occurs with amplitude $G_{k,\ell}$.

B. Properties of an individual XX chain

It is instructive to stop briefly to review some of the basic properties of a single XX chain, for instance that described by the Hamiltonian H_1 in Eq. (49). The eigenvalues of H_1 are divided in bands (subspaces) containing specific numbers of b-fermions. The first band contains a single state corresponding to no b-fermions. Its energy is $E_0 = 0$ and we refer to it as the vacuum, $|0\rangle$. It can be shown that $|0\rangle = |-\rangle^{\otimes N}$, the factored state where all spins are pointing down. Next there are a series of N states corresponding to 1 b-fermion with energies λ_k and eigenstates $|k\rangle = b_k^\dagger |0\rangle$. This is followed by a series of $\binom{N}{2}$ states with energy $\lambda_{k_1} + \lambda_{k_2}$ where, to avoid double counting, we adopt the convention that $k_2 > k_1$. The corresponding eigenstates are defined as $|k_1 k_2\rangle = b_{k_2}^\dagger b_{k_1}^\dagger |0\rangle$. In general, the subspace with p b-fermions has energy $\lambda_{k_1} + \dots + \lambda_{k_p}$ and eigenvectors

$$|k_1, \dots, k_p\rangle = b_{k_p}^\dagger \dots b_{k_1}^\dagger |0\rangle$$

where $k_p > k_{p-1} > \dots > k_1$. In total the system has

$$1 + \binom{N}{1} + \binom{N}{2} + \binom{N}{3} + \dots + \binom{N}{N} = 2^N$$

possible states, as expected.

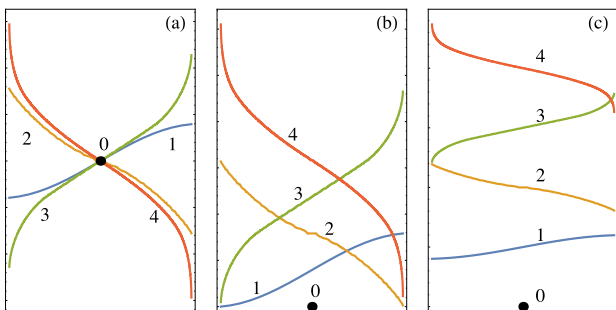


FIG. 1. Diagram of the first few energy bands containing different numbers of b-fermions for $N = 20$. The horizontal axis has no physical meaning and the number of states is different in each band. (a) $h = 0$. (b) $h = h_f = 2 \cos\left(\frac{\pi}{N+1}\right) \simeq 1.98$. (c) $h = 10$.

In Fig. 1 we present diagrams of the first few energy bands corresponding to different numbers of b-fermions

for $N = 20$ and different values of h . Here and henceforth, in all numerical calculations, we shall set $J = 1$. At $T = 0$ the quantum XX chain is known to undergo a quantum phase transition [63] at the *factorizing field*

$$h_f = 2J \cos\left(\frac{\pi}{N+1}\right) \simeq 2J \quad (53)$$

When $h \geq h_f$ the ground state will be the vacuum $|0\rangle$ with energy $E_0 = 0$. As mentioned, this corresponds to all spins aligned with the magnetic field. Conversely, when $|h| \leq h_f$, the ground state will have an energy smaller than zero. For instance, if $h = 0$ the ground state energy is $-2JN/\pi$. The two situations are illustrated in Figs. 1(a) and (b) for $h = 0$ and $h = h_f$ respectively. Increasing h above the factorizing field will also lead to the appearance of band gaps in the first few levels of the energy spectrum, as shown in Fig. 1(c) for $h = 10$. This will be important for our future discussion since the probabilities of work and heat in Eqs. (25) and (33) depend on the thermal probabilities p_n defined in Eq. (9). If h is sufficiently large, the thermal occupation numbers for higher bands will be negligible compared to those of the first few bands.

Now that we have diagonalized H_1 , it is straightforward to compute equilibrium thermodynamic quantities since quadratic forms of Fermionic operators commute. If we let T be the temperature of the chain, then the partition function is

$$Z = \text{tr}(e^{-H_1/T}) = \prod_{k=1}^N (1 + e^{-\lambda_k/T}) \quad (54)$$

The average occupation number is given by the Fermi-Dirac distribution

$$\bar{n}_k(T) = \langle b_k^\dagger b_k \rangle = \frac{1}{e^{\lambda_k/T} + 1} \quad (55)$$

and the internal energy is

$$U(T) = \langle H_1 \rangle = \sum_{k=1}^N \lambda_k \langle b_k^\dagger b_k \rangle = \sum_{k=1}^N \frac{\lambda_k}{e^{\lambda_k/T} + 1} \quad (56)$$

In the thermodynamic limit we may write $x = \pi k/(N+1)$ and transform this sum into an integral; viz,

$$U(T) = \frac{N}{\pi} \int_0^\pi \frac{\lambda(x)}{e^{\lambda(x)/T} + 1} dx \quad (57)$$

where

$$\lambda(x) = h + 2J \cos(x) \quad (58)$$

This is illustrated in Fig. 2(a) and (b). At $T = 0$ the internal energy coincides with the ground state. It is negative for $h < h_f$ and zero otherwise. This is a clear manifestation of the quantum phase transition. When $T \neq 0$,

the internal energy changes smoothly, even though the general trend is similar to the case $T = 0$.

It is also interesting to compute the specific heat since, according to Eq. (2), if $T_2 = T_1 + \Delta T$ and ΔT is small, then the total heat exchanged between the two systems will be

$$Q \simeq \frac{C(T)}{2} \Delta T \quad (59)$$

We have

$$C(T) = \frac{\partial U}{\partial T} = \frac{N}{\pi} \int_0^\pi \frac{\lambda^2}{T^2} \frac{e^{\lambda/T}}{(e^{\lambda/T} + 1)^2} dx \quad (60)$$

The results for $C(T)$ are shown in Fig. 2(c) and (d). These curves give a measure of the magnitude of the total heat transferred. Note how, at low temperatures, the specific heat is suppressed above the factorizing field. This is a consequence of the appearance of band gaps in the energy band.

The average density of b-fermions is defined as

$$\bar{n} = \frac{1}{N} \sum_{k=1}^N \bar{n}_k(T) = \frac{1}{\pi} \int_0^\pi \frac{1}{e^{\lambda(x)/T} + 1} dx \quad (61)$$

The behavior of \bar{n} is shown in Fig. 2(e) and is somewhat similar to $U(T)$. For $T = 0$ it is non-zero at $h < h_f$ and becomes identically zero at $h \geq h_f$.

The system is not translationally invariant, so that the magnetization $\langle \sigma_i^z \rangle$ changes from one site to the other. Notwithstanding, we may define the average magnetization per particle as

$$\bar{m} = \frac{1}{N} \sum_{k=1}^N \langle \sigma_i^z \rangle \quad (62)$$

Due to the fact that the $x_{k,\ell}$ form an orthogonal matrix, it follows that

$$\bar{m} = 2\bar{n} - 1 = -\frac{1}{\pi} \int_0^\pi \tanh \left[\frac{\lambda(x)}{2T} \right] dx \quad (63)$$

Thus, Fig. 2(e) also corresponds to a plot of the magnetization. It starts at 0 when $h = 0$ and changes continuously toward -1 when $h = h_f$. Finally, the susceptibility is

$$\chi = \frac{N}{\pi T} \int_0^\pi \text{sech}^2 \left[\frac{\lambda(x)}{2T} \right] dx \quad (64)$$

This is presented in Fig. 2(f). For $T = 0$ it diverges exactly at $h = h_f$, whereas for finite T this divergence is transformed into a peak whose sharpness diminishes with increasing temperature.

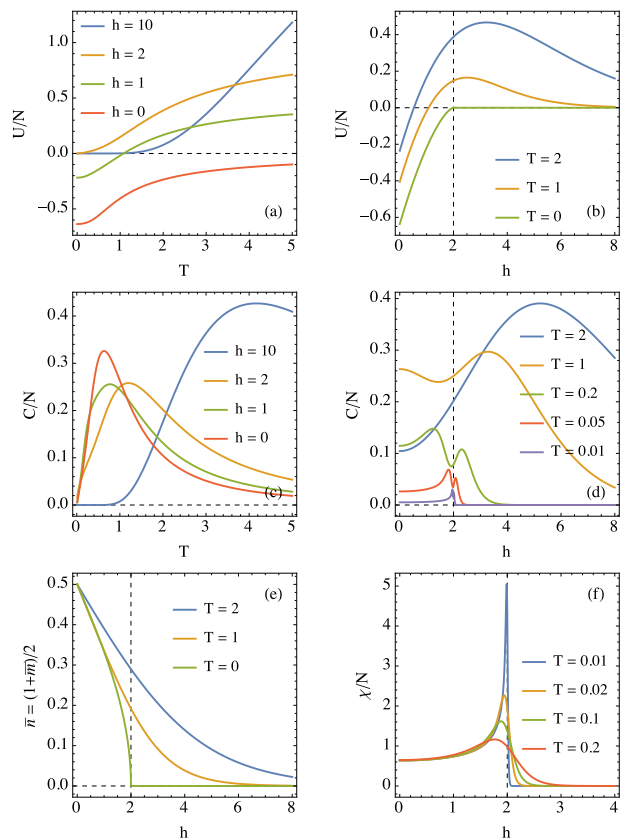


FIG. 2. Equilibrium properties of the quantum XX chain in the thermodynamic limit. (a) Internal energy per spin U/N vs. T for different values of h . (b) Same but as a function of h . The vertical line corresponds to $h_f = 2J$. (c) and (d) Similar to (a) and (b) but for the specific heat. (e) Density of b-fermions $\bar{n} = (1 + \bar{m})/2$ vs. h . (f) Susceptibility χ/N vs. h .

IV. PERTURBATIVE SOLUTION

The Hamiltonians H_1 and H_2 in Eqs. (49) and (50) clearly commute with the operator counting the total number of b-fermions in the two chains combined, $\sum_{k=1}^{2N} b_k^\dagger b_k$. The same is true for V since each term in Eq. (51) creates a b-fermion in one chain and destroys a b-fermion in the other. Hence, the time evolution under the total Hamiltonian $H = H_1 + H_2 + V$ preserves the total number of b-fermions. This strongly restricts the number of allowed transitions in the computation of the distributions of work or heat, Eqs. (25) and (33) respectively. Notwithstanding, the number of transitions remains enormous and the task thus remains formidable.

We shall therefore adopt a different approach, based on perturbation theory. Note that the potential V in Eq. (51) depends on

$$g = \frac{2g_0}{N+1} \quad (65)$$

which will be small if either g_0 is small or N is large. We may thus treat V as a perturbation with small parameter

g . The accurateness of this approximation should then improve as the size of the systems increase. In particular, first order perturbation theory should become *exact* in the thermodynamic limit, irrespective of the actual value of g_0 .

Using Eqs. (49), (50) and (51) we may write the total Hamiltonian $H = H_1 + H_2 + V$ as

$$H = \sum_{k,\ell=1}^{2N} R_{k,\ell} b_k^\dagger b_\ell \quad (66)$$

where

$$R = \begin{bmatrix} \Lambda & G \\ G^T & \Lambda \end{bmatrix} \quad (67)$$

in which G is the $N \times N$ matrix with entries $G_{k,\ell}$ defined in Eq. (52) and

$$\Lambda = \text{diag}(\lambda_1, \dots, \lambda_N)$$

Since H is still quadratic in Fermionic operators, we may apply to it the same procedure used to diagonalize H_1 and H_2 , based on orthogonal transformations [cf. Eq. (47)]. Even though this may be performed exactly, it will lead to an extremely cumbersome result which is of little practical use.

Instead, what we shall do is first apply perturbation theory to the matrix R assuming that g is a small parameter, and then diagonalize H using orthogonal transformations. Let us denote the basis elements in which Eq. (67) was written as $|k, 0\rangle$ and $|0, k\rangle$, where $k = 1, \dots, N$. That is,

$$R|k, 0\rangle = \lambda_k |k, 0\rangle + \sum_{\ell=1}^N G_{k,\ell} |0, \ell\rangle$$

$$R|0, k\rangle = \lambda_k |0, k\rangle + \sum_{\ell=1}^N G_{\ell,k} |\ell, 0\rangle$$

If $g = 0$ each pair $\{|k, 0\rangle, |0, k\rangle\}$ will be doubly degenerate with eigenvalue λ_k . The presence of g lifts this degeneracy, causing a splitting of the levels. We may therefore use degenerate perturbation theory to find the new eigenvalues and eigenvectors. According to the standard recipe [68], we must compute the matrix elements of the perturbed part of R in the 2-dimensional subspaces spanned by the vectors $\{|k, 0\rangle, |0, k\rangle\}$. In our case these matrix elements are

$$\begin{bmatrix} 0 & G_k \\ G_k & 0 \end{bmatrix}$$

where

$$G_k = G_{k,k} = (-1)^{k+1} g \sin^2 \left(\frac{\pi k}{N+1} \right) \quad (68)$$

Thus, the perturbed eigenvalues to first order in g are $\lambda_k \pm G_k$ and the new eigenvectors are $\frac{|k,0\rangle \pm |0,k\rangle}{\sqrt{2}}$.

Inserting these results into H in Eq. (66) we obtain

$$H = \sum_{k=1}^N B_k \quad (69)$$

where

$$B_k = \lambda_k (b_k^\dagger b_k + b_{k+N}^\dagger b_{k+N}) + G_k (b_k^\dagger b_{k+N} + b_{k+N}^\dagger b_k) \quad (70)$$

If we compare this with Eq. (51) we see that, physically, this equation means that to first order in g , the only meaningful transitions in V are those which destroy a b-fermion in one chain and create a b-fermion in the other, *with the same energy*. Hence, these are transitions which retain no energy in the interaction term, which is precisely what is expected within the context of the Jarzynski and Wójcik fluctuation theorem [11].

The operators B_k in Eq. (69) commute,

$$[B_k, B_\ell] = 0 \quad (71)$$

Moreover, B_k commutes with any Fermionic quadratic form with indices $\ell \neq k$. These facts are the key to compute all quantities of interest. They mean that the dynamics, which in general occurs in the space of $2N$ b-fermions, factors into N subspaces containing only 2 b-fermions.

Before we turn to the actual distributions of heat and work, let us illustrate how this procedure may be implemented to find the density matrix at time t ,

$$\rho(t) = U(t) \rho_{\text{th}} U^\dagger(t) \quad (72)$$

Both the time evolution operator and the initial thermal states may be factored as products:

$$U(t) = \prod_{k=1}^N e^{-iB_k t}$$

and

$$\rho_{\text{th}} = \prod_{k=1}^N \frac{e^{-\beta_1 \lambda_k b_k^\dagger b_k - \beta_2 \lambda_k b_{k+N}^\dagger b_{k+N}}}{(1 + e^{-\beta_1 \lambda_k})(1 + e^{-\beta_2 \lambda_k})}$$

Hence the density matrix will also factor as a product of N terms:

$$\rho(t) = \prod_{k=1}^N \rho_k(t) = \prod_{k=1}^N \frac{e^{-iB_k t} e^{-\beta_1 \lambda_k b_k^\dagger b_k - \beta_2 \lambda_k b_{k+N}^\dagger b_{k+N}} e^{iB_k t}}{(1 + e^{-\beta_1 \lambda_k})(1 + e^{-\beta_2 \lambda_k})} \quad (73)$$

Each term in this product now lives in a 4×4 subspace spanned by the vectors

$$\begin{aligned} |0, 0\rangle \\ |k, 0\rangle &= b_k^\dagger |0, 0\rangle \\ |0, k\rangle &= b_{k+N}^\dagger |0, 0\rangle \\ |k, k\rangle &= b_{k+N}^\dagger b_k^\dagger |0, 0\rangle \end{aligned}$$

In this subspace the reduced time-evolution operator $e^{-iB_k t}$ is, apart from a complex phase $e^{-i\lambda_k t}$,

$$e^{-iB_k t} = \begin{bmatrix} e^{i\lambda_k t} & 0 & 0 & 0 \\ 0 & \cos(G_k t) & -i \sin(G_k t) & 0 \\ 0 & -i \sin(G_k t) & \cos(G_k t) & 0 \\ 0 & 0 & 0 & e^{-i\lambda_k t} \end{bmatrix} \quad (74)$$

Performing the product in Eq. (73) we therefore conclude that the density matrix $\rho_k(t)$ is

$$\rho_k(t) = \frac{1}{Z_k} \begin{bmatrix} 1 & 0 & 0 & 0 \\ 0 & p_1 & -iq & 0 \\ 0 & iq & p_2 & 0 \\ 0 & 0 & 0 & e^{-(\beta_1 + \beta_2)\lambda_k} \end{bmatrix} \quad (75)$$

where

$$Z_k = (1 + e^{-\beta_1 \lambda_k})(1 + e^{-\beta_2 \lambda_k}) \quad (76)$$

$$p_1 = e^{-\beta_1 \lambda_k} \cos^2(G_k t) + e^{-\beta_2 \lambda_k} \sin^2(G_k t) \quad (77)$$

$$p_2 = e^{-\beta_2 \lambda_k} \cos^2(G_k t) + e^{-\beta_1 \lambda_k} \sin^2(G_k t) \quad (78)$$

$$q = (e^{-\beta_2 \lambda_k} - e^{-\beta_1 \lambda_k}) \cos(G_k t) \sin(G_k t) \quad (79)$$

In the following sections we will apply this same approach to compute all thermodynamic quantities of interest.

V. THE STATISTICS OF WORK

We begin with the statistics of the work performed by the external agent in turning on the interaction. This very same problem was studied recently in Ref. [62]. In that case the probabilities were computed numerically using exact diagonalization. Consequently, only small sizes were accessible.

In this particular problem the average work defined in Eq. (21) is zero:

$$\langle W \rangle = \langle V \rangle_0 = 0 \quad (80)$$

Since all time evolution operators factor into smaller subspaces, the characteristic function defined in Eq. (26) can be factored into a product of N traces acting on the subspaces of two b-fermions:

$$M(u) = \prod_{k=1}^N \frac{\text{tr} \left\{ e^{iuB_k} e^{-(\beta_1 + iu)\lambda_k} b_k^\dagger b_k - (\beta_2 + iu)\lambda_k b_{k+N}^\dagger b_{k+N} \right\}}{Z_k}$$

These terms may be computed using Eq. (74) and the same approach of the previous section. The result is

$$M(u) \prod_{k=1}^N \frac{1 + e^{-(\beta_1 + \beta_2)\lambda_k} + (e^{-\beta_1 \lambda_k} + e^{-\beta_2 \lambda_k}) \cos(G_k u)}{Z_k} \quad (81)$$

For the particular case where $\beta_1 = \beta_2 = \beta$ this simplifies to

$$M(u) = \prod_{k=1}^N \frac{\cosh(\beta \lambda_k) + \cos(G_k u)}{\cosh(\beta \lambda_k) + 1} \quad (82)$$

The fact that the characteristic function may be written as a product of N terms makes it much more tractable analytically than $P(W)$.

To compute $P(W)$ we must perform the inverse Fourier transform of $M(u)$. Suppose we expand the product in Eqs. (81) or (82) in terms of complex exponentials in u obtaining

$$M(u) = \sum_a \Gamma_a e^{iuw_a}$$

for coefficients Γ_a and w_a . Applying the inverse Fourier transform we therefore obtain

$$P(W) = \Gamma_a \delta(W - w_a) \quad (83)$$

Analyzing the structure of Eqs. (81) or (82) we conclude that the allowed values of W are, in this case,

$$\begin{aligned} & \pm G_k \\ & \pm G_{k_1} \pm G_{k_2} \\ & \pm G_{k_1} \pm G_{k_2} \pm G_{k_3} \end{aligned}$$

etc., with no repeated indices. Each term above may be traced back to the energy band diagrams in Fig. 1. A value of the work which is a sum of p terms of the form $\pm G_k$ corresponds to a transition where the initial and the final state had p b-fermions in the two chains combined (recall that transitions between bands are not allowed). The bookkeeping is not so trivial, however, since the G_k [cf. Eq. (68)] may be either positive or negative. Moreover, it is necessary to account for an enormous number of degeneracies. In any case, the maximum value of W is

$$\sum_{k=1}^N |G_k| = g_0$$

which is physically very intuitive.

We now illustrate the distribution of work $P(W)$ in various situations. For simplicity, we shall focus on the case $\beta_1 = \beta_2 = \beta$. In what concerns the distribution of work, this is not a restrictive assumption.

The method described in Eq. (83) may be used to compute $P(W)$ when the size N is small. Otherwise it becomes prohibitively expensive. In Fig. 3 we present a comparison between the exact work distribution computed using Eq. (25) and the approximate solution obtained from Eq. (83) for the case $N = 4$, $h = 1$, $T = 2$ and $g_0 = 0.01$. When the distribution is computed exactly and g_0 is small, there is a tendency for the probabilities to aggregate in clusters. The perturbative solution

does not account for this, treating all points as one. For this reason we see in Fig. 3(a) a clear disagreement between the two solutions. However, this is only an artifact related to the fact that g_0 is small but not infinitesimal. To compare the two solutions we may group the probabilities of each cluster of the exact solution. The result is shown in Fig. 3(b) where, as can be seen, the agreement is excellent.

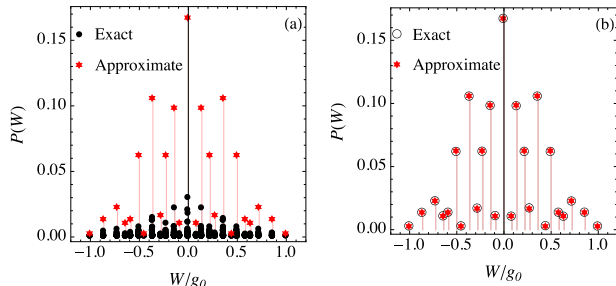


FIG. 3. Comparison between the approximate work distribution computed using Eq. (83) and the exact result computed using Eq. (25). The parameters are $N = 4$, $h = 1$, $T = 2$ and $g_0 = 0.01$. (a) Raw results. (b) Grouping terms in the exact solution which are sufficiently close to each other.

The number of allowed values of W increases exponentially with N . Hence, in order to find $P(W)$ for large sizes it becomes necessary to use the Fast Fourier Transform (FFT) algorithm [69] directly in Eq. (81) or (82). It should be pointed out, however, that this leads only to a coarse-grained description of $P(W)$. For very large N , though, the results should become increasingly more accurate.

We begin with the case of high temperatures. Results for $N = 200$ are shown in Fig. 4. Each image corresponds to a different temperature, starting at $T = 10$ and going down to $T = 2$. Moreover, each curve correspond to a different value of h , from 0 to 8 in steps of 1. At high temperatures the curves are practically not affected by the magnetic field. This is reasonable since the magnetic field redistributes the energy bands in Fig. 1 and at high temperatures this practically does not affect the thermal populations. Conversely, for large fields, if we reduce the temperature, the populations of the upper levels get depleted, leading to a sharpening of the probability distribution (recall that higher bands contribute to larger values of W).

As the temperature is reduced further the effects of the quantum phase transition at $h = h_f \simeq 2$ become more salient. In this case it becomes essential to analyze the interplay between T and h . In the limit of $h \rightarrow \infty$ the only populated level would be the vacuum, in which case no work would ever be performed. Hence, in this case we expect that $P(W = 0) = 1$. On the other hand, for zero field, even at low temperatures, it is very easy to populate the different energy bands. Therefore, the distribution of work should be spread over many possible values leading to $P(W = 0) \simeq 0$. This is somewhat similar than what

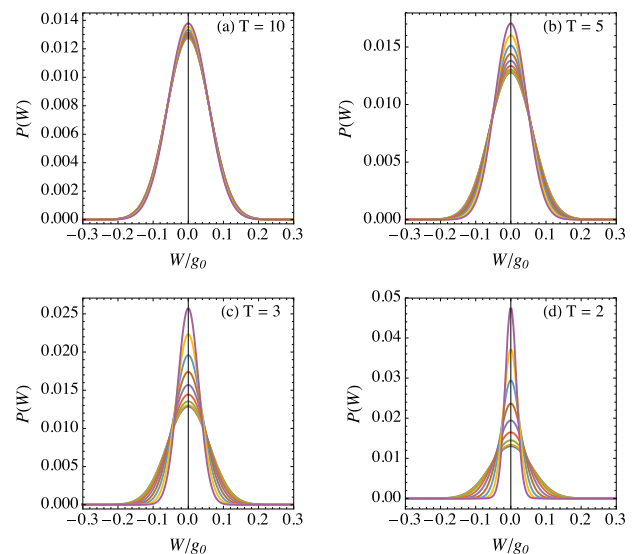


FIG. 4. Work distribution for high temperatures and $N = 200$ computed using FFT. Each image corresponds to a different temperature, as indicated in the labels. Moreover, each curve correspond to different values of h , ranging from $h = 0$ (lowermost, when viewed at the peak) to $h = 8$ (uppermost) in unit steps.

happens in Bose-Einstein condensation, in which for high temperatures the population is spread over a continuum of states but at low temperatures they accumulate on one specific state. As h is varied one therefore expects an abrupt transition between these two regimes. This is illustrated in Fig. 5 where we plot $P(W = 0)$ (also computed from FFT) as a function of h for different values of T and $N = 400$. For finite temperatures the transition is smooth and occurs for $h > h_f$. However, as $T \rightarrow 0$ the transition tends to a discontinuity at $h = h_f$.

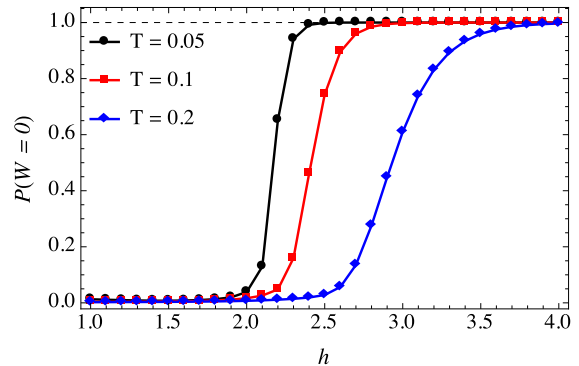


FIG. 5. The probability that no work is performed, $P(W = 0)$, vs. h for different temperatures with $N = 400$ and $g_0 = 0.1$.

Lastly, we discuss in more detail the distribution of work for low temperatures and fields below h_f (above h_f all probability is concentrated at $W = 0$). In Fig. 6 we

present $P(W)$ for $T = 0.1$ and 0.2 and different values of h with $N = 400$. It is seen that at very low temperatures and $h = 0$ the distribution acquires sharp peaks, which are destroyed when h is increased. The origin of these peaks can be understood as follows. If $h = 0$ and N is even the ground state of each chain occurs in the band with $N/2$ b-fermions. Therefore, as $T \rightarrow 0$, the distribution of work will have contributions only from transitions which started in this specific band. At finite h , on the other hand, the ground state becomes a mixing of many energy bands, which consequentially lead to a smoother form for $P(W)$.

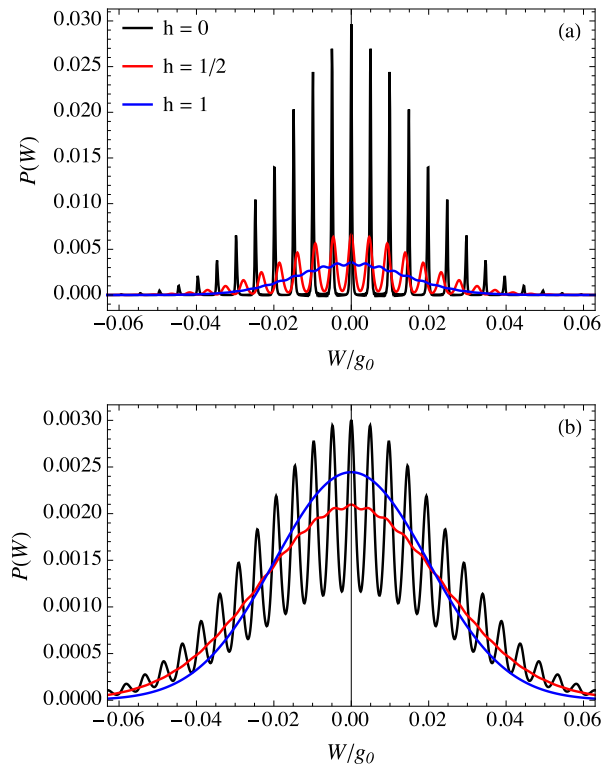


FIG. 6. $P(W)$ for (a) $T = 0.1$ and (b) $T = 0.2$ with $N = 400$ and different values of h , as indicated.

VI. AVERAGE HEAT

Before studying the distribution $P_t(Q)$ we consider first the average heat defined in Eq. (22). The average occupation numbers as a function of time may be computed using Eq. (75). They read

$$\langle b_k^\dagger b_k \rangle_t = \bar{n}_k(T_1) \cos^2(G_k t) + \bar{n}_k(T_2) \sin^2(G_k t)$$

$$\langle b_{k+N}^\dagger b_{k+N} \rangle_t = \bar{n}_k(T_2) \cos^2(G_k t) + \bar{n}_k(T_1) \sin^2(G_k t)$$

We now need simply to insert these results into Eq. (22), using also Eqs. (49) and (50). It follows, as expected, that

in the current approximation $\langle Q_1 \rangle_t = -\langle Q_2 \rangle_t := \langle Q \rangle_t$, where

$$\langle Q \rangle_t = \sum_{k=1}^N \lambda_k [\bar{n}_k(T_2) - \bar{n}_k(T_1)] \sin^2(G_k t) \quad (84)$$

Notice that the average heat evolves with a characteristic relaxation time

$$\tau = \frac{1}{g} = \frac{N+1}{2g_0} \quad (85)$$

Thus, the relaxation time scales with the linear dimensions of the system, exactly as expected from classical thermodynamics [60]. Note also that this is the only place where the constant g_0 appears in the result. We shall henceforth always measure time in units of τ , which therefore eliminates any dependence on g_0 .

We begin by analyzing the transition from small to large system sizes. In Figs. 7 and 8 we present $\langle Q \rangle_t/N$ vs. gt for several sizes, with $T_1 = 2$ and $T_2 = 3$ and for $h = 0$ and $h = 10$ respectively. In each figure the horizontal dashed line corresponds to the equilibrium heat \mathcal{Q} expected from thermodynamics, Eq. (2). As can be observed, for small sizes the average heat oscillates violently around \mathcal{Q} . As the size increases one gradually observes the existence of two distinct regimes. For small times the heat behaves in an orderly fashion, either as a practically monotonically increasing function of time, as in Fig. 7, or as an oscillatory function as in Fig. 8. In either case, these curves are seen to gradually tend to the expected thermodynamic value \mathcal{Q} as $t \rightarrow \infty$. However, in all situations a time always comes where violent oscillations start and never size. These oscillations are a signature of finite size effects and appear for all combinations of parameters. Hence, we conclude that *finite systems never thermalize*.

On the other hand, it is also possible to observe in Figs. 7 and 8 that the moment where these oscillations start increases with the size of the system. In fact, it is possible to assert from the numerical analysis that this transition is proportional to N^2 , in contrast with the relaxation time which scales linearly with N . Consequently, we expect that *in the thermodynamic limit, the systems do thermalize*. Indeed, for N sufficiently large we may replace the sum in Eq. (84) by an integral, exactly like was done in going from Eq. (56) to Eq. (57). The result is

$$\langle Q \rangle_t = \frac{N}{\pi} \int_0^\pi \lambda(x) [\bar{n}(x, T_2) - \bar{n}(x, T_1)] \sin^2(gt \sin^2 x) dx \quad (86)$$

where $\lambda(x)$ is defined in Eq. (58) and

$$\bar{n}(x, T) = (e^{\lambda(x)/T} + 1)^{-1}$$

The extensive nature of $\langle Q \rangle_t$ is made evident in this formula. Since Eq. (84) was computed using as perturbation

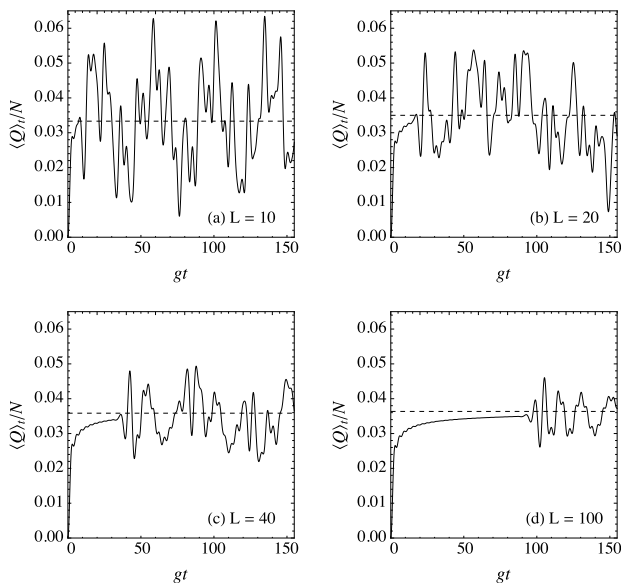


FIG. 7. $\langle Q \rangle_t / N$ vs. gt for several sizes, as indicated, with $T_1 = 2$, $T_2 = 3$ and $h = 0$. The horizontal dashed lines correspond to Q/N computed from Eq. (2).

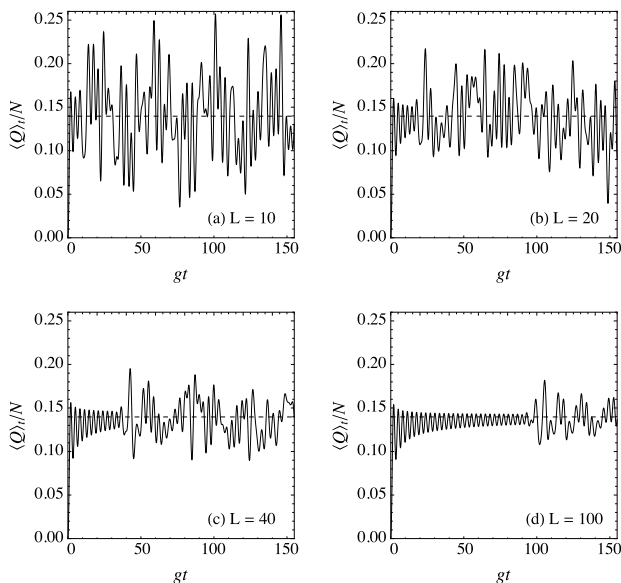


FIG. 8. Same as Fig. 8 but for $h = 10$.

parameter the quantity $2g_0/(N+1)$, its accuracy should improve with increasing system size. Hence, we conclude that Eq. (86) is an *exact result* for the average heat exchanged in the thermodynamic limit, irrespective of the size of the interaction term g_0 (provided, of course, that g_0 does not depend on N).

When $gt \rightarrow \infty$ the term $\sin^2(gt \sin^2 x)$ will oscillate infinitely fast between its limits 0 and 1 as x is changed from 0 to π in the integral of Eq. (86). Hence, we may

replace it by its average value 1/2. The result is

$$\langle Q \rangle_{t \rightarrow \infty} = \frac{N}{\pi} \int_0^\pi \lambda(x) \frac{[\bar{n}(x, T_2) - \bar{n}(x, T_1)]}{2} dx$$

This is precisely the thermodynamic value for the exchanged heat Q in Eq. (2) [see also Eq. (57)]. Thus, we conclude that *in the thermodynamic limit the two chains always thermalize*.

Further examples of the average heat for various sizes are shown in Figs. 9 and 10. The manifestation of the thermodynamic limit is evident in these figures: in all cases, the violent oscillations are always shifted to larger times as the size increase. Before these oscillations start, the curves for different sizes coincide precisely. In Fig. 10 it is also possible to observe the manifestation of the quantum phase transition: the heat exchanged for $h = 10$ (image (c)) is approximately 10 orders of magnitude smaller than that of image (b) where $h = 1$. According to Fig. 1, such a large magnetic field leads to large band gaps which in turn strongly hinder the thermal populations of upper levels.

It is also possible to compute the average heat using a different method, which also allow us to compare our approximate solution with exact simulations. Define the covariance matrix

$$\theta_{k,\ell} = \langle b_k^\dagger b_\ell \rangle \quad (87)$$

where $k, \ell = 1, \dots, 2N$. From the von Neumann equation it can be shown that the matrix θ satisfies

$$\frac{d\theta}{dt} = i[R, \theta] \quad (88)$$

where the matrix R is the same as that given in Eq. (67). The initial conditions of Eq. (88) correspond to the two chains being separately prepared in thermal equilibrium at temperatures T_1 and T_2 . According to Eq. (55) this means that

$$\theta_{k,k}(0) = \bar{n}_k(T_1), \quad \theta_{k+N,k+N}(0) = \bar{n}_k(T_2) \quad (89)$$

for $k = 1, \dots, N$. The formal solution of Eq. (88) is

$$\theta(t) = e^{iRt} \theta(0) e^{-iRt} \quad (90)$$

It is possible to apply the same perturbative analysis used before directly to Eq. (90). This results, as is expected, in the same formula for $\langle Q \rangle_t$ shown in Eq. (84). Alternatively, we may simulate Eq. (90) directly since all it requires is the diagonalization of the $2N \times 2N$ matrix R . This yields a numerically exact method that may be used to test the accuracy of the present approximation. An example of such a comparison is shown in Fig. 11 for $N = 100$ and $N = 200$. As can be seen, both solutions are practically indistinguishable. In the highly oscillatory part, a phase difference is developed between the two, which is due to the higher order terms neglected

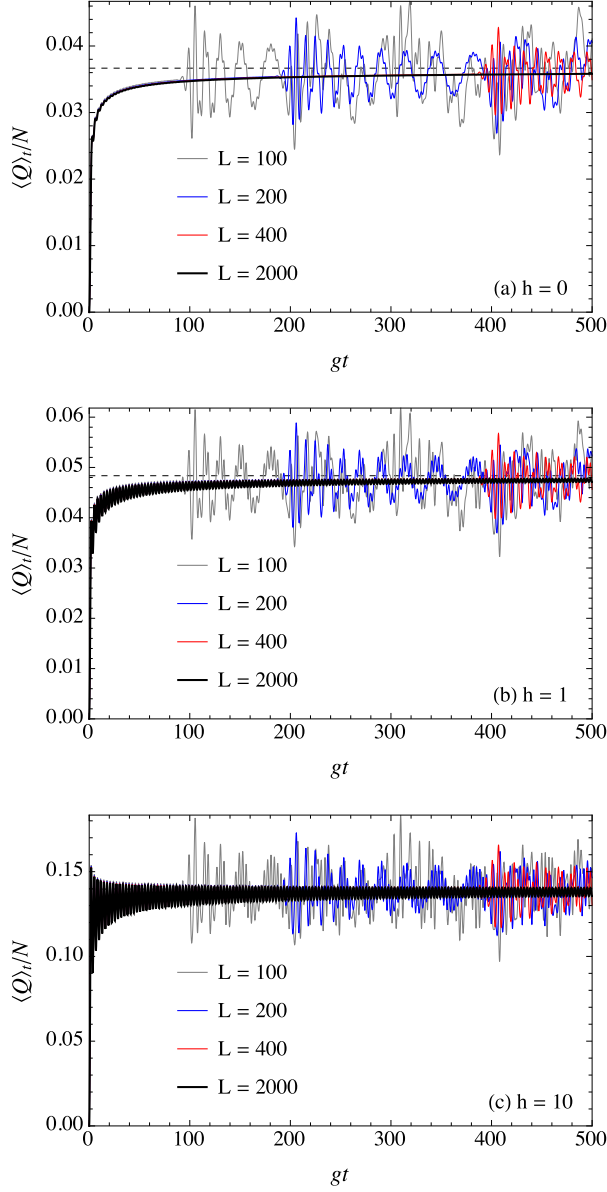


FIG. 9. $\langle Q \rangle_t / N$. vs. gt for different sizes and different values of h (as shown in each figure) for $T_1 = 2$ and $T_2 = 3$.

in the perturbative analysis. Notwithstanding, it is seen that as the size increases, the agreement between the two solutions improves. Thus, as argued before, the accuracy of the perturbative approach improves with N and becomes exact in the thermodynamic limit.

We now investigate in more detail the properties of $\langle Q \rangle_t$ in the thermodynamic limit [Eq. (86)] at very low temperatures, where the quantum phase transition should play an important role. In Fig. 12 we present the average heat below the factorizing field for $T_1 = 0.01$ and $T_2 = 0.02$. At these temperatures, the only meaningful excitations comes from states close to the ground state of the two chains. The lower the magnetic field,

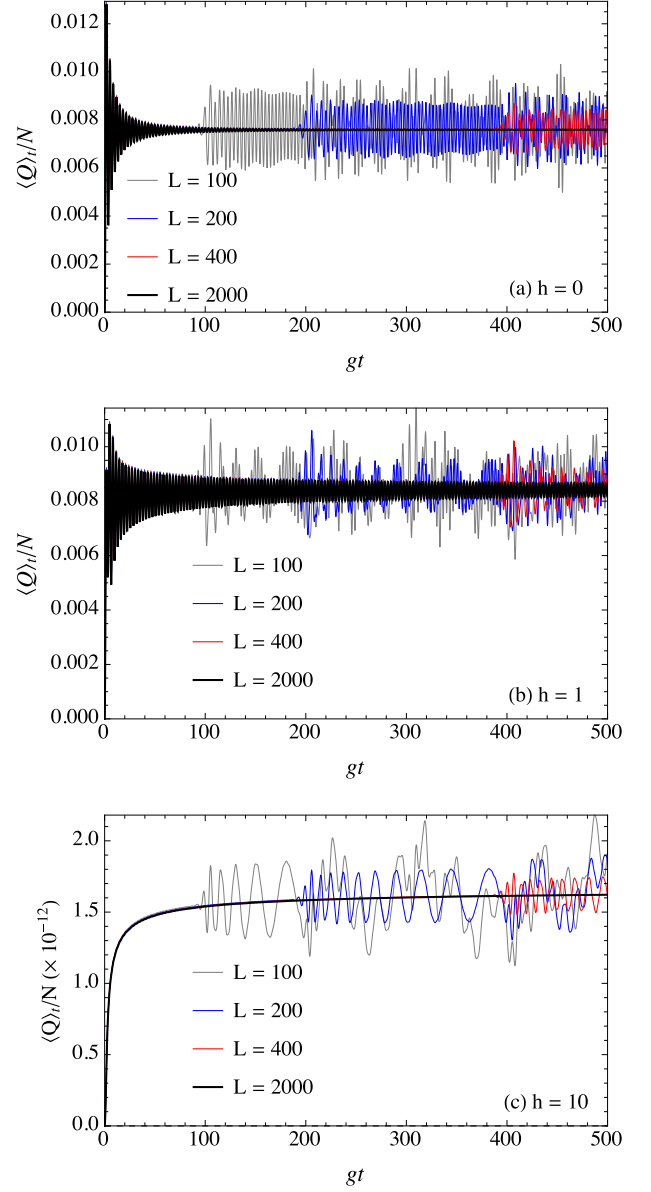


FIG. 10. Same as Fig. 9 but for low temperatures, $T_1 = 0.2$ and $T_2 = 0.3$.

the more oscillatory is $\langle Q \rangle_t$ since more states can be accessed. Conversely, as h increases the energy levels are all shifted upwards, which leads to a damping of these oscillations. For $h \geq h_f$ these oscillations are replaced by an over-damped behavior.

Another case of interest is that of $h = 0$. Results for different values of T_1 , with fixed $T_2 = T_1 + 0.01$, in the thermodynamic limit, are presented in Fig. 13. In this case the temperature acts as a damping for the average heat. In the limit $T_{1,2} \rightarrow 0$ the average heat would oscillate indefinitely and never thermalize, even in the thermodynamic limit. For finite temperatures, however, the oscillations are damped and the systems eventually

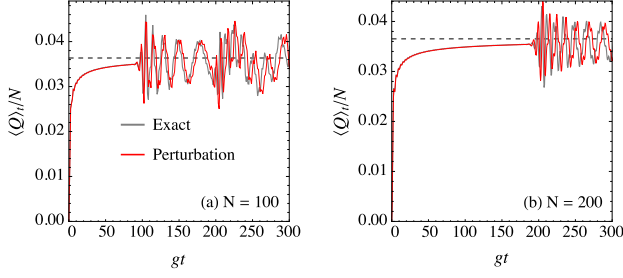


FIG. 11. Comparison between the approximate solution, Eq. (84) and the numerically exact solution computed from Eq. (90) for two different sizes, with $h = 10$, $T_1 = 2$, $T_2 = 3$ and $g_0 = 0.15$.

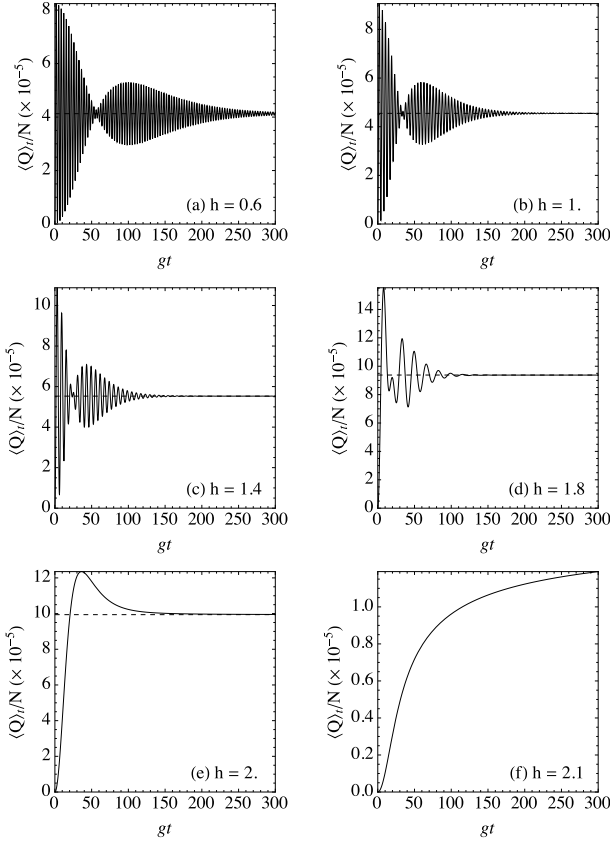


FIG. 12. $\langle Q \rangle_t / N$ vs. gt in the thermodynamic limit for $T_1 = 0.01$, $T_2 = 0.02$ and different values of h .

thermalize. As the temperature increases we also observe the transition from an oscillatory to a monotonically increasing behavior.

VII. STATISTICS OF HEAT

Finally we arrive at the distribution of heat $P_t(Q)$ defined in Eq. (33). As in the statistics of work, it is intractable to compute $P_t(Q)$ exactly, even within our ap-

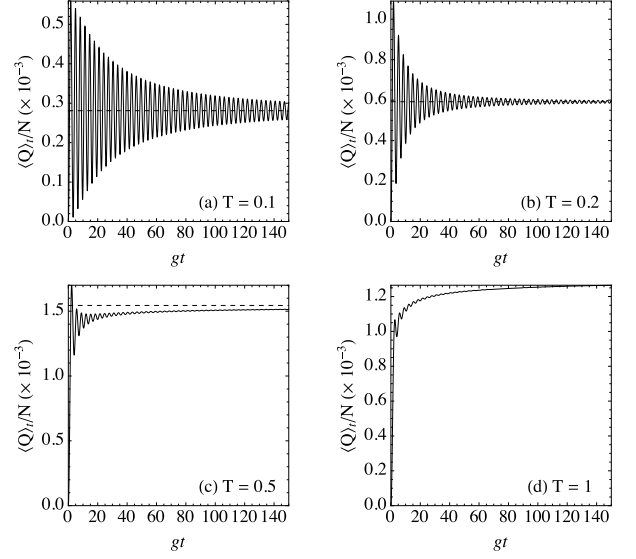


FIG. 13. $\langle Q \rangle_t$ vs. gt in the thermodynamic limit for $h = 0$ and different values of T_1 with fixed $T_2 = T_1 + 0.01$.

proximations. The problem is again one of bookkeeping. Instead, we compute the characteristic function defined in Eq. (34). As before, this function factors into a product of traces acting on 4×4 subspaces and which may be computed using Eq. (74). The final result is

$$F_t(r) = \prod_{k=1}^N [1 + f_k(r) \sin^2(G_k t)] \quad (91)$$

where

$$f_k(r) = \frac{(e^{ir\lambda_k} - 1)e^{-\lambda_k/T_2} + (e^{-ir\lambda_k} - 1)e^{-\lambda_k/T_1}}{Z_k} \quad (92)$$

with Z_k defined in Eq. (76). It can be verified that this formula satisfies the non-equilibrium equality in Eq. (4) by setting $r = i\Delta\beta = i(\beta_1 - \beta_2)$. Consequently, $P_t(Q)$ will satisfy the Jarzynski and Wójcik fluctuation theorem in Eq. (3). It is also worth noting that the asymmetry of $P_t(Q)$ when $\beta_1 \neq \beta_2$ is manifested in the fact that $F_t(r)$ is in general complex. It only becomes real when $\beta_1 = \beta_2$.

The analysis in this case is similar to that of the average work in Sec. V. When we expand the product in Eq. (91) we will obtain several terms of the form e^{irq_a} , which then correspond to the allowed values of Q . These values are in fact the combinations λ_k , $\lambda_k \pm \lambda_\ell$, etc. For small N we may perform this expansion exactly, in order to compare the perturbative analysis with the exact solution. Results for $N = 4$ are shown in Fig. 14 for two different values of h . The agreement with the exact solution is noteworthy. Please also note that the vertical axis is in log scale.

In order to find $P_t(Q)$ for large sizes we must invert Eq. (91) numerically using the FFT algorithm. It should

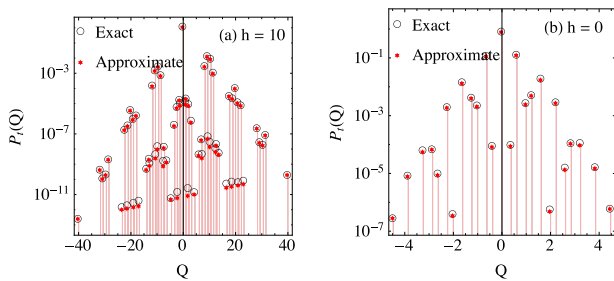


FIG. 14. Comparison between the exact heat distribution and the perturbative solution computed using Eq. (91), for $N = 4$, $T_1 = 2$, $T_2 = 3$, $g_0 = 0.1$ and $t = 15$. (a) $h = 10$ and (b) $h = 0$.

again be remarked, however, that this procedure is only coarse grained and is unable to capture the fine structure of $P_t(Q)$. Notwithstanding, it is possible to test the accurateness of this method by computing the first two moments of Q and comparing with exact expressions. In all cases presented here, the accuracy was of at least one part in a million.

In Fig. 15 we present the distributions of heat for $N = 100$ at a specific time $gt = 30$. The situation is similar to those presented in Fig. 7(d) and 8(d), namely $T_1 = 2$ and $T_2 = 3$, with different values of h . As can be seen, for low fields the distribution is broadened by increasing h . However, for sufficiently large fields we begin to observe the appearance of certain sharp peaks together with a strong concentration of probability at $Q = 0$. This is a manifestation of the quantum phase transition and is similar to what was observed in the distribution of work. In image (f), for $h = 10$, the probability $P(Q = 0)$ is already roughly 0.1.

Next we turn to the time dependence of the probability distribution. There are several combinations of parameters, specially at high temperatures, which lead to a somewhat uninteresting behavior resembling a Gaussian distribution whose position oscillates with time. We consider instead the low temperature behavior and focus on $h < h_f$ since, otherwise, the probability would be all concentrated at $Q = 0$. Fig. 16 shows the probability of heat $P_t(Q)$ computed at several instants of time for $N = 100$, $h = 0$, $T_1 = 0.5$ and $T_2 = 0.7$. The inset in each image shows the average heat as a function of gt and the particular moment where the distribution was computed. The behavior of $P_t(Q)$ shown in Fig. 16 is extremely rich. For most values of t , the distribution has a smooth Gaussian shape. However, during certain intervals of time it is possible to observe the appearance of sharp peaks together with a concentration of probability at $Q = 0$. After some time these peaks disappear, only to reappear again at a later time, albeit with a smaller amplitude. Hence, as the time progresses, this raggedness becomes less and less pronounced, which is accompanied by a damping of the oscillations of $\langle Q \rangle_t$.

It is interesting to note that effects such as those ob-

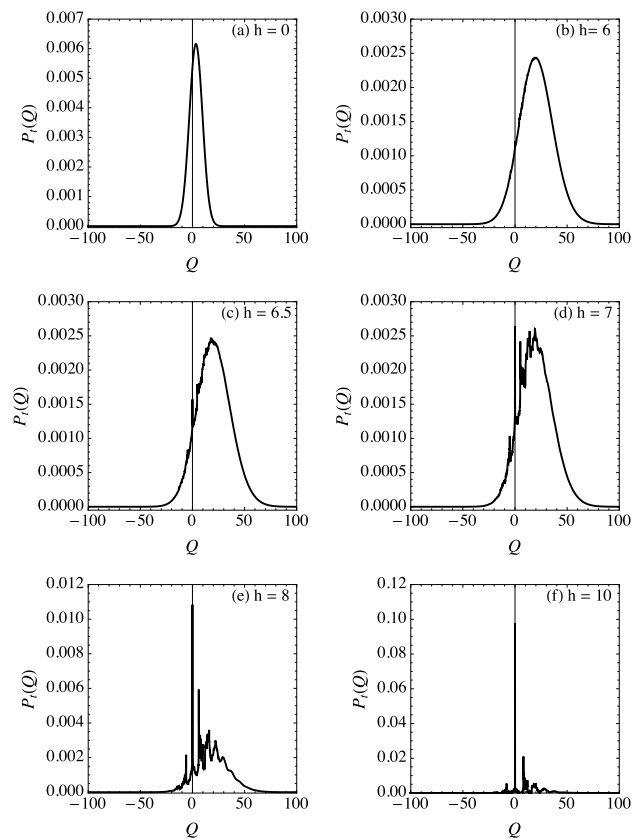


FIG. 15. $P_t(Q)$ for $gt = 30$, $N = 100$, $T_1 = 2$, $T_2 = 3$ and different values of h , as shown in each image.

served in Fig. 16 do not appear at the “unstable” part of the average heat. In fact, these instabilities manifest themselves in a subtle way in terms of the probability distribution. This will be discussed in more detail below.

From the previous discussion it can be concluded that, just like the distribution of work, in the case of heat it is essential to distinguish between the continuum of values that Q may take and the case $Q = 0$ which, at some cases, may have a substantial probability. Thus we now analyze the probability that no heat is transferred, $P_t(Q = 0)$. This may be computed from Eq. (91) by collecting all terms which are independent of r . Unlike in the work distribution, where the values G_k are oscillatory, here the λ_k are monotonically increasing functions of k . Hence, terms which depend on r will never be zero for specific combinations of the indices. With this in mind it is possible to obtain, after a careful arrangement of the terms, that

$$P(Q = 0) = \prod_{k=1}^N \left[1 - \frac{(e^{-\lambda_k/T_1} + e^{-\lambda_k/T_2})}{Z_k} \sin^2(G_k t) \right] \quad (93)$$

This equation is illustrated in Fig. 17 as a function of time for $N = 100$ and different values of h and T_1 . At $t = 0$ we obviously have $P(Q = 0) = 1$. As time progresses, this probability tends to diminish and the rate

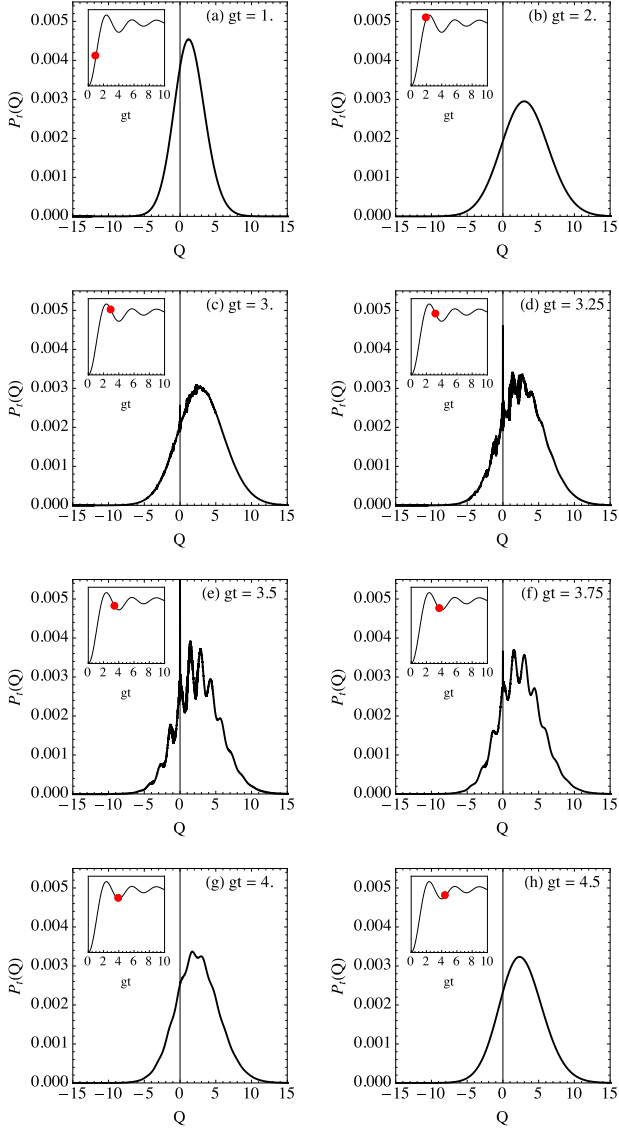


FIG. 16. $P_t(Q)$ for several instants of time (as denoted in each image) for $N = 100$, $h = 0$, $T_1 = 0.5$ and $T_2 = 0.7$. The insets show the average heat as a function of time and the instant at which each distribution was computed.

at which it does depends on the temperature and the magnetic field. In all images we see a drastic transition around the factorizing field $h_f = 2$. In Fig. 17(a), when $h < h_f$ the curves decay quickly to zero whereas if $h > h_f$ they present a fast initial decay followed by a much slower trend. As the temperature is reduced, we start to observe resonant oscillations below the factorizing field, which become very pronounced at low temperatures. Conversely, for $h > h_f$ the low temperature curves remain at $P_t(Q = 0) = 1$ for all times, similarly to what was observed in the distribution of work.

Finally, we turn to the topic of understanding how the violent finite-size fluctuations of the average heat are manifested in terms of the probabilities $P_t(Q)$. It turns

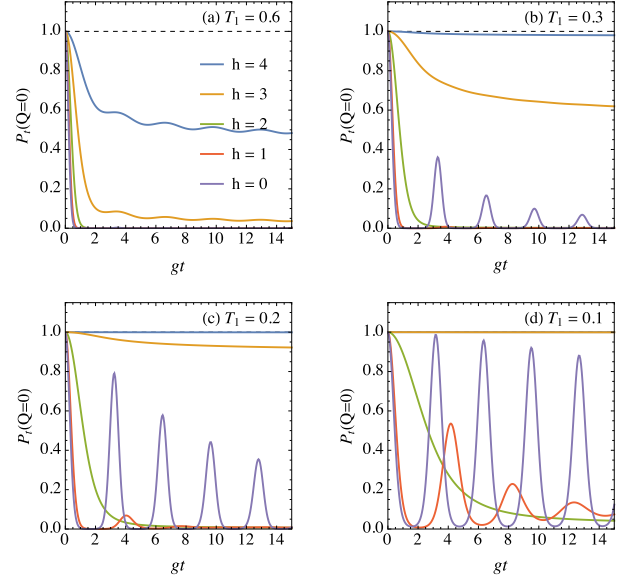


FIG. 17. Probability of no heat flowing, $P_t(Q = 0)$ as a function of time for $N = 100$ and different values of T_1 and h , with fixed $T_2 = T_1 + 0.02$.

out, however, that this manifestation is a rather subtle effect which cannot be captured by the FFT method since it is, by definition, only coarse-grained. Thus, in order to proceed, we will consider a rather special situation in which we are capable of finding $P_t(Q)$ exactly. The situation corresponds to that shown in Fig. 10(c), where the temperatures are low ($T_1 = 0.2$ and $T_2 = 0.3$) and the field is large ($h = 10$), well above h_f . The corresponding band structure is shown in Fig. 1(c). If we compute $P_t(Q)$ using the FFT we obtain the result shown in Fig. 18, in which $gt = 50$ and $N = 400$. As can be seen, practically all probability is concentrated in $Q = 0$. The only part which remains is a small cluster of probability around the interval $8 \leq Q \leq 12$. We will now show that the probabilities in this cluster may be computed exactly and through them we will be able to understand the oscillations of the average heat.

The large magnetic field induces a sizable band gap between the first few levels. In addition, the low temperatures guarantee that the thermal occupation numbers p_n of the higher bands will be exponentially suppressed. In this case we may only consider those transitions in Eq. (33) in which the system originally had only one b-fermion in the two chains combined. Let $|k, 0\rangle$ denote the state where chain 1 has a b-fermion of energy λ_k and chain 2 has no b-fermions, and similarly for $|0, k\rangle$. Then there are only two possibilities. In the first, chain 1 started with zero b-fermions and, at a time t , gained a b-fermion with energy λ_k . This corresponds to a transition of the form $|0, k\rangle \rightarrow |k, 0\rangle$ and the total heat which entered system 1 is $Q = \lambda_k$. The second possibility is the opposite situation yielding $Q = -\lambda_k$.

These probabilities may be computed either directly

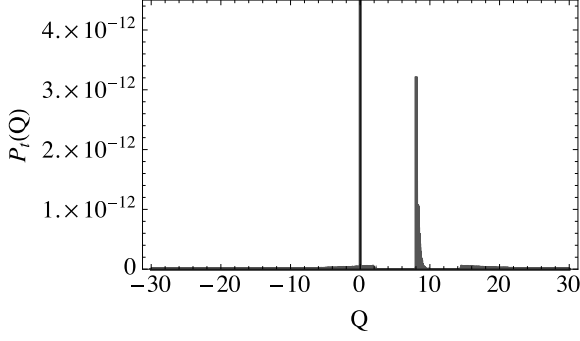


FIG. 18. $P_t(Q)$ for $T_1 = 0.2$, $T_2 = 0.3$, $h = 10$, $N = 400$ and $gt = 50$ computed using FFT.

from Eq. (33) or from the characteristic function in Eq. (91). The latter method is more straightforward since it only involves expanding the product and retaining only the first order terms. Note that, since h is large, $\lambda_k \geq 0$ so that $e^{-\beta\lambda_k}$ is always a small quantity. The result is

$$P(Q = \lambda_k) = \frac{e^{-\lambda_k/T_2}}{Z_k} \sin^2(G_k t) \quad (94)$$

$$P(Q = -\lambda_k) = \frac{e^{-\lambda_k/T_1}}{Z_k} \sin^2(G_k t) \quad (95)$$

Of course, we also have $P(Q = 0)$ which, in fact, is practically one. Given the definition of λ_k in Eq. (45) we therefore conclude that either Q will be in the interval $[h - 2J, h + 2J]$, which is what can be seen in Fig. 18, or it will be in the opposite interval $[-2J - h, 2J - h]$. The reason why this interval does not appear in Fig. 18 is that Eq. (95) depends exponentially on the temperature and $T_1 < T_2$. It is also worth noting that the probabilities in Eqs. (94) and (95) clearly satisfy the fluctuation theorem in Eq. (3). Moreover, the value of $\langle Q \rangle_t$ which they give agrees with Eq. (84) provided we expand $(e^{\beta\lambda_k} + 1)^{-1} \simeq e^{-\beta\lambda_k}$.

We will focus only on the positive interval of heat described by Eq. (94). The results as a function of time for $T_1 = 0.2$, $T_2 = 0.3$, $h = 10$ and $N = 400$ are shown in Fig. 19. See also the videos in the supplemental material. As can be seen, when the average heat approaches the “unstable” region, certain gaps appear in the probabilities followed by probability fluxes between the different regions. In Fig. 20 we show the same situation, but now analyzed for the thermodynamic limit. It can be seen that these gaps are no longer present, leading to a smooth curve which is oscillatory but whose frequency increases with time. As $t \rightarrow \infty$ this tends to a compact distribution of an exponential shape. We therefore conclude that the violent finite-size oscillations in the average heat are related to instabilities in the probability distribution and the appearance of unstable probability fluxes.

Lastly, we discuss the probability of second law viola-

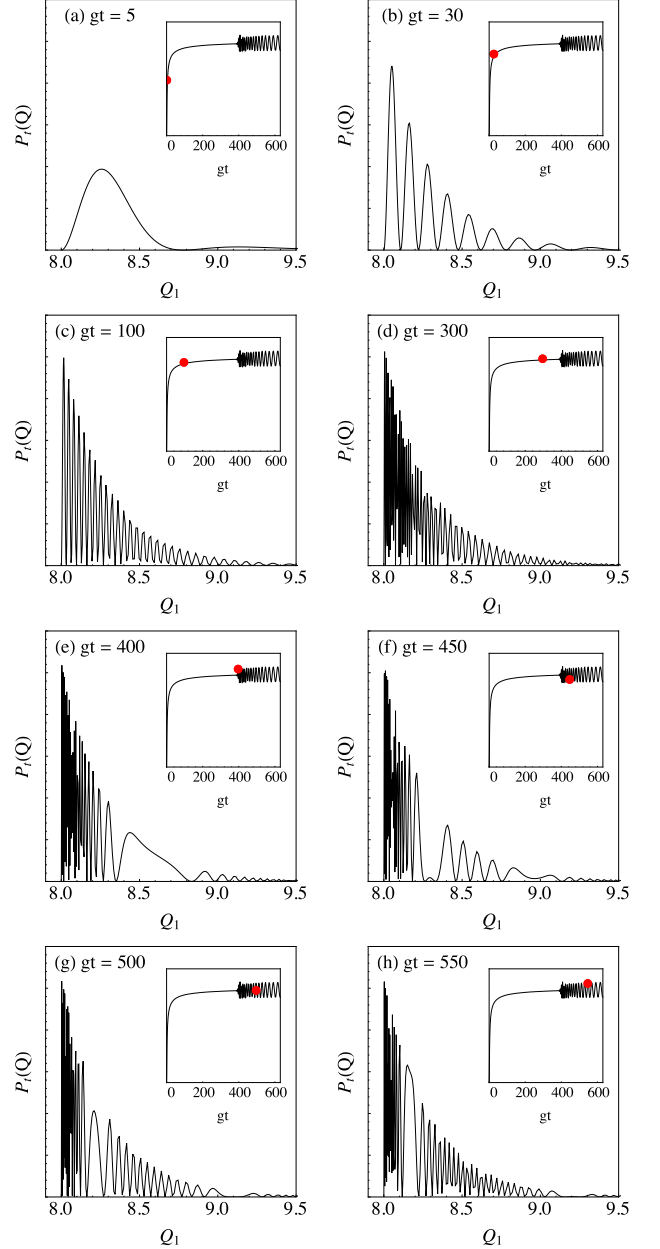


FIG. 19. Probabilities $P_t(Q_1)$ for different instants of time for the same situation of Fig. 10(c); namely $N = 400$, $h = 10$, $T_1 = 0.2$ and $T_2 = 0.3$.

tions $P_t(Q < 0)$. This may be computed either from FFT or from Eq. (36). In Fig. 21 we show $P_t(Q < 0)$ for several situations focusing on $h = 0$. In images (a) and (b) we consider the case of fixed $T_1 = 1$ and $T_2 = T_1 + \Delta T$, and study $P_t(Q < 0)$ as a function of ΔT for different values of N and vice-versa. As expected, the larger the temperature difference, the smaller is the probability of obtaining negative heat. A similar trend is obtained as a function of N . In Fig. 21(c) we study $P_t(Q < 0)$ as a function of time for different values of T_1 with fixed $\Delta T = 0.1$. It is found that $P_t(Q < 0)$ oscillates with

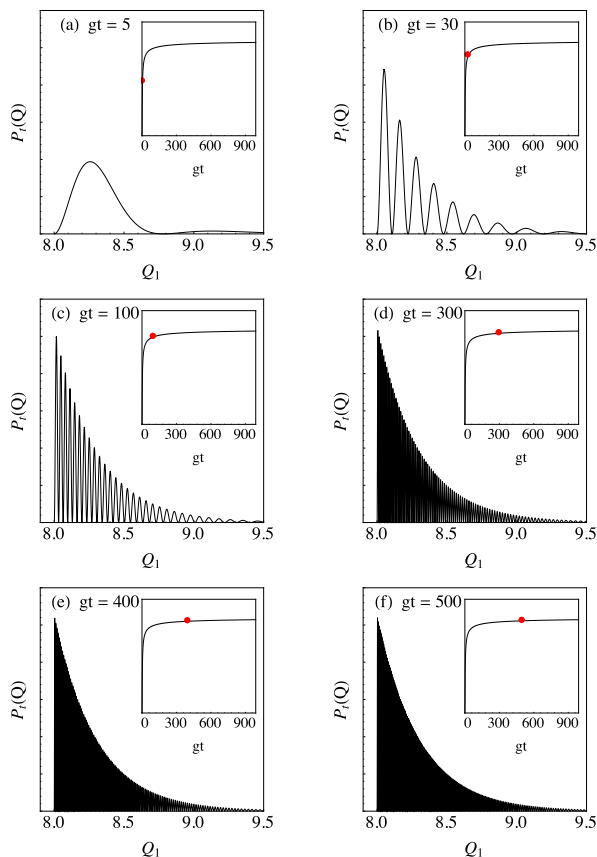


FIG. 20. Probabilities $P_t(Q_1)$ for different instants of time in the thermodynamic limit, with $h = 10$, $T_1 = 0.2$ and $T_2 = 0.3$.

time, the oscillations being more pronounced at lower temperatures. Finally, in Fig. 21(d) we look at the effect of increasing h . In this case care must be taken in analyzing the results since there is an accumulation of probability at $Q = 0$. It is for this reason that, as we increase h , we observe a step rise in $P(Q < 0)$ (in this case it would be better interpreted as $P(Q \leq 0)$).

VIII. CONCLUSIONS

In this paper I studied the statistics of heat and work in the connection of two quantum spin chains which were initially prepared at different temperatures. The main idea was to develop a perturbative approach that would enable us to understand this type of non-equilibrium situation for arbitrary sizes. I then provided a lengthy investigation of how the size and, in particular, the thermo-

dynamic limit, affect the fluctuations of thermodynamic quantities. The method developed here is readily extensible to other many-body quantum systems and may also work as a starting point to analyze interacting systems, such as for instance the XXZ chain. Another point worth noting is the important effect that the quantum phase transition has on all thermodynamic quantities. In fact, it leads to a plethora of different, and extremely rich, phenomena. It is my hope that this discussion contributed to our current understanding of non-equilibrium fluctuation relations and how they manifest themselves in quantum many-body systems.

ACKNOWLEDGMENTS

I acknowledge the São Paulo Research Foundation (FAPESP) for the financial support. Moreover, I am thankful to Pedro Gomes, Mario José de Oliveira, Roberto Serra, Fernando Semião, Mauro Paternostro, John Goold and Eric Lutz, for fruitful discussions.

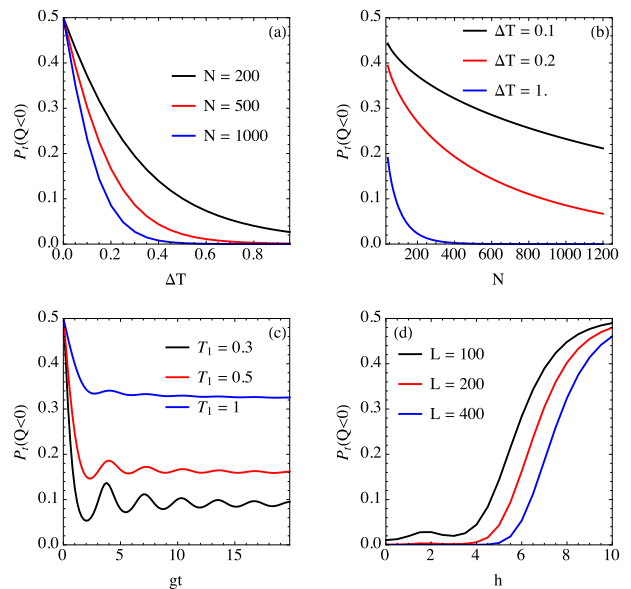


FIG. 21. Probability of second law violations, $P_t(Q < 0)$, in different situations for $h = 0$ (except image (d)). (a) As a function of ΔT for different values of N , where $T_1 = 1$, $T_2 = T_1 + \Delta T$ and $gt = 50.0$. (b) As a function of N for different values of ΔT , again with $T_1 = 1$ and $gt = 50.0$. (c) As a function of time for $N = 400$, $\Delta T = 0.1$ and different values of T_1 . (d) Effect of changing h on $P(Q < 0)$ for $T_1 = 0.5$, $T_2 = 1$ and $gt = 50$.

- [1] A. del Campo, J. Goold, and M. Paternostro, *Scientific Reports* **4**, 6208 (2014).
 [2] T. B. Batalhão, A. M. Souza, R. S. Sarthour, I. S. Oliveira, M. Paternostro, E. Lutz, and R. M. Serra,

arXiv:1502.06704v1.

- [3] D. J. Evans, E. G. D. Cohen, and G. P. Morriss, *Physical Review Letters* **71**, 2401 (1993); D. J. Evans and D. J. Searles, *Physical Review E* **50**, 1645 (1994);

- Advances in Physics **51**, 1529 (2002); S. Williams, D. J. Searles, and D. J. Evans, Physical Review Letters **100**, 250601 (2008); D. J. Evans, S. R. Williams, and D. J. Searles, The Journal of chemical physics **134**, 204113 (2011).
- [4] G. Gallavotti and E. G. D. Cohen, Journal of Statistical Physics **80**, 931 (1995); Physical Review Letters **74**, 2694 (1995).
- [5] D. A. Sivak and G. E. Crooks, Physical Review Letters **108**, 150601 (2012).
- [6] G. E. Crooks, Journal of Statistical Physics **90**, 1481 (1998); Physical Review E **61**, 2361 (2000); Journal of Statistical Mechanics: Theory and Experiment **2008**, P10021 (2008).
- [7] C. Jarzynski, Physical Review E **56**, 5018 (1997); Physical Review Letters **78**, 2690 (1997); Journal of statistical physics **96**, 415 (1999); Journal of Statistical Physics **98**, 77 (2000); Proceedings of the National Academy of Sciences **98**, 3636 (2001); Annual Review of Condensed Matter Physics **2**, 329 (2011).
- [8] J. Kurchan, Journal of Physics A: Mathematical and General **31**, 3719 (1998).
- [9] C. Maes, Journal of Statistical Physics **95**, 367 (1999).
- [10] J. Lebowitz and H. Spohn, Journal of Statistical Physics **95**, 333 (1999).
- [11] C. Jarzynski and D. K. Wójcik, Physical Review Letters **92**, 230602 (2004).
- [12] J. Hoppenau and A. Engel, Journal of Statistical Mechanics: Theory and Experiment **2013**, P01004 (2013).
- [13] N. A. Sinitsyn, Journal of Physics A: Mathematical and Theoretical **44**, 405501 (2011).
- [14] H. Tasaki, (2000), arXiv:0009244 [cond-mat].
- [15] J. Kurchan, (2000), arXiv:0007360 [cond-mat].
- [16] S. Mukamel, Physical Review Letters **90**, 170604 (2003), arXiv:0302190 [cond-mat].
- [17] T. Monnai, Physical Review E **72**, 027102 (2005).
- [18] J. Teifel and G. Mahler, Physical Review E **76**, 051126 (2007); Physical Review E **83**, 041131 (2011).
- [19] P. Talkner, E. Lutz, and P. Hänggi, Physical Review E **75**, 050102 (2007); P. Talkner, M. Campisi, and P. Hänggi, Journal of Statistical Mechanics: Theory and Experiment **2009**, P02025 (2009); P. Talkner, M. Morillo, J. Yi, and P. Hänggi, New Journal of Physics **15**, 095001 (2013).
- [20] M. F. Gelin and D. S. Kosov, Physical Review E **78**, 011116 (2008).
- [21] S. Vaikuntanathan and C. Jarzynski, EPL (Europhysics Letters) **87**, 60005 (2009).
- [22] M. Esposito, Reviews of Modern Physics **81**, 1665 (2009).
- [23] M. Campisi, P. Hänggi, and P. Talkner, Reviews of Modern Physics **83**, 771 (2011).
- [24] D. Cohen and Y. Imry, Physical Review E **86**, 011111 (2012).
- [25] M. Olshani, Physical Review Letters **114**, 060401 (2015).
- [26] R. Chetrite and K. Mallick, Journal of Statistical Physics **148**, 480 (2012).
- [27] J. Goold, M. Paternostro, and K. Modi, Physical Review Letters **114**, 060602 (2015).
- [28] R. van Zon, S. Ciliberto, and E. Cohen, Physical Review Letters **92**, 130601 (2004).
- [29] F. Douarche, S. Ciliberto, a. Petrosyan, and I. Rabbiosi, Europhysics Letters (EPL) **70**, 593 (2005).
- [30] J. R. Gomez-Solano, A. Petrosyan, and S. Ciliberto, Physical Review Letters **106**, 200602 (2011).
- [31] S. Ciliberto, A. Imparato, A. Naert, and M. Tanase, Physical Review Letters **110**, 180601 (2013).
- [32] T. B. Batalhão, A. M. Souza, L. Mazzola, R. Auccaise, R. S. Sarthour, I. S. Oliveira, J. Goold, G. De Chiara, M. Paternostro, and R. M. Serra, Physical Review Letters **113**, 140601 (2014).
- [33] J. Ren, P. Hänggi, and B. Li, Physical Review Letters **104**, 170601 (2010).
- [34] J. Hide and V. Vedral, Physical Review A **81**, 062303 (2010).
- [35] S. Rahav, U. Harbola, and S. Mukamel, Physical Review A **86**, 043843 (2012).
- [36] S. Deffner and C. Jarzynski, Physical Review X **3**, 041003 (2013).
- [37] D. B. Witort, C. Jarzynski, S. B. Smith, I. Tinoco, and C. Bustamante, Nature **437**, 231 (2005).
- [38] I. Bena, C. V. D. Broeck, and R. Kawai, Europhysics Letters (EPL) **71**, 879 (2005).
- [39] R. Cleuren, C. Van den Broeck, and R. Kawai, Physical Review E **74**, 021117 (2006); B. Cleuren and C. V. D. Broeck, Europhysics Letters (EPL) **79**, 30001 (2007).
- [40] G. Crooks and C. Jarzynski, Physical Review E **75**, 021116 (2007).
- [41] C. Chatelain, Journal of Physics A: Mathematical and General **2007**, P04001 (2007); Journal of Statistical Mechanics: Theory and Experiment **2007**, P04001 (2007).
- [42] S. Dorosz, T. Platini, and K. Karevski, Physical Review E **77**, 051120 (2008).
- [43] F. Corberi, G. Gonnella, and A. Pelizzola, Journal of Statistical Mechanics: Theory and Experiment **2009**, P01004 (2009).
- [44] R. Dorner, J. Goold, C. Cormick, M. Paternostro, and V. Vedral, Physical Review Letters **109**, 160601 (2012).
- [45] F. Cornu and M. Bauer, Journal of Statistical Mechanics: Theory and Experiment **2013**, P10004 (2013).
- [46] M. Brunelli, A. Xuereb, A. Ferraro, G. De Chiara, N. Kiesel, and M. Paternostro, (2014), arXiv:1412.4803.
- [47] K. Saito and A. Dhar, Physical Review Letters **99**, 180601 (2007).
- [48] L. Nicolin and D. Segal, Physical Review B **84**, 161414 (2011).
- [49] A. Kundu, S. Sabhapandit, and A. Dhar, Journal of Statistical Mechanics: Theory and Experiment **2011**, P03001 (2011).
- [50] G. Y. Panasyuk, G. A. Levin, and K. L. Yerkes, Physical Review E **86**, 021116 (2012).
- [51] H. C. Fogedby, Journal of Physics A: Mathematical and Theoretical **47**, 325003 (2014).
- [52] A. Piscitelli, F. Corberi, and G. Gonnella, Journal of Physics A: Mathematical and Theoretical **41**, 332003 (2008).
- [53] Y. Sughiyama and S. Abe, Journal of Statistical Mechanics: Theory and Experiment **2008**, P05001 (2008).
- [54] F. Corberi, G. Gonnella, A. Piscitelli, and M. Zannetti, Journal of Physics A: Mathematical and Theoretical **46**, 042001 (2013).
- [55] S. Lahiri and A. Jayannavar, (2013), arXiv:1312.4677v1.
- [56] S. Gasparinetti, P. Solinas, A. Braggio, and M. Sassetti, New Journal of Physics **16**, 115001 (2014).
- [57] B. K. Agarwalla, H. Li, B. Li, and J.-S. Wang, Physical Review E **89**, 052101 (2014).
- [58] K. Kim, C. Kwon, and H. Park, Physical Review E **90**, 032117 (2014).
- [59] J. Goold, U. Poschinger, and K. Modi, Physical Review E **90**, 020101 (2014).
- [60] H. B. Callen, *Thermodynamics and an introduction to Thermostatistics*, 2nd ed. (Wiley, 1985) p. 493.
- [61] R. Landauer, Journal of Statistical Physics **13**, 1 (1975).
- [62] T. J. G. Apollaro, G. Francica, M. Paternostro, and M. Campisi, (2014), arXiv:1406.0648.

- [63] T. Niemeijer, *Physica* **36**, 377 (1967).
- [64] L. Fusco, S. Pigeon, T. J. G. Apollaro, A. Xuereb, L. Mazzola, M. Campisi, A. Ferraro, M. Paternostro, and G. De Chiara, *Physical Review X* **4**, 13 (2014).
- [65] M. Girardeau, *Journal of Mathematical Physics* **1**, 516 (1960)
- [66] T. Kinoshita, T. Wenger, and D. S. Weiss, *Science* **305**, 1125 (2004).
- [67] R. Jedicke, D. Nesvorný, R. Whiteley, Z. Ivezić Z, and M. Jurić, *Nature* **429**, 275 (2004).
- [68] K. Gottfried and T.-M. Yan, *Quantum mechanics: fundamentals*, 2nd ed. (Springer, 2004).
- [69] W. H. Press, S. A. Teukolsky, W. T. Vetterling, and B. P. Flannery, *Numerical Recipes*, 3rd ed. (Cambridge University Press, New York, 2007).